NATURAL SCIENCE REVIEW 3 100703 (2026)
nsr.jinr.int

Giant dipole resonance and related spin-dependent excitations

E. B. Balbutsev[1] and I. V. Molodtsova*[1]

[1] *Joint Institute for Nuclear Research, 141980 Dubna, Russia*

Abstract

The time-dependent Hartree–Fock equation is solved by the Wigner function moments method taking into account spin degrees of freedom. Energies and reduced transition probabilities of $K^\pi = 0^-$, 1^- and 2^- excitations are calculated taking ^{164}Dy as an example. The spin degrees of freedom give rise to the electric spin dipole resonance. Its properties and interplay with the giant dipole resonance are investigated. The deformation-induced splitting of the spin $M2$ resonance is discussed. The results of calculations are compared with the experimental data and other theoretical studies.

Keywords: collective motion, giant dipole resonance, spin dipole resonances

DOI: 10.54546/NaturalSciRev.100703

1. Introduction

Collective nuclear dynamics is among the most interesting topics of experimental and theoretical research. The Wigner Function Moments (WFM) method is an effective tool for describing collective motion in atomic nuclei (and any other multiparticle systems). The solution of the time-dependent Hartree–Fock–Bogolyubov equations by the WFM method made it possible to find the energies and excitation probabilities of giant resonances (isoscalar and isovector quadrupole, isoscalar (compression) and isovector dipole) and various low-lying modes. The nuclear collective motion of the rotational type (scissors modes) was studied in the series of papers [1–8]. It was shown that additionally to the conventional nuclear scissors mode there can exist the pair of scissors modes connected with the nucleons spin degrees of freedom. They appear due to the spin-orbit part of the nucleus mean field. The conventional scissors mode is generated by the out-of-phase rotational oscillations of neutrons with respect to protons, whereas two spin modes are generated by the analogous motion of all "spin-up" nucleons with respect to all "spin-down" nucleons. These three modes are classified as isovector spin-scalar, isovector spin-vector and isoscalar spin-vector ones. Now it would be quite natural to investigate the nonrotational motions for the possible existence of the proper spin excitations, for example, the spin giant resonances of various multipolarities.

*Corresponding author e-mail address: molod@theor.jinr.ru

Received: 23 January 2026; Revised: 13 April 2026; Accepted: 20 April 2026; Published: 15 May 2026

In this paper we consider the Giant Dipole Resonance (GDR) and related spin-dependent excitations. The systematics of the GDR is by now well established [9, 10]. At the same time, the knowledge about spin-dependent excitations of negative parity remains rather limited, both experimental and theoretical, see [11–16].

We already studied 1^- excitations in the papers [17, 18], where the Time-Dependent Hartree–Fock (TDHF) equation was solved by the WFM method taking into account the moments of first and third ranks. The calculations were performed with Skyrme forces neglecting by the deformation of nuclei and by spin degrees of freedom. Orbital 2^- excitations were also studied in this approach [19].

The results for the 1^- excitations are reproduced in Figures 1 and 2. The theory produced seven energy levels (Fig. 1). The centroid of two of them describes very well the position of GDR energy centroid (Fig. 2). The simplified calculations, without third rank moments, produce only one level. It is marked by a dotted line in Figure 2.

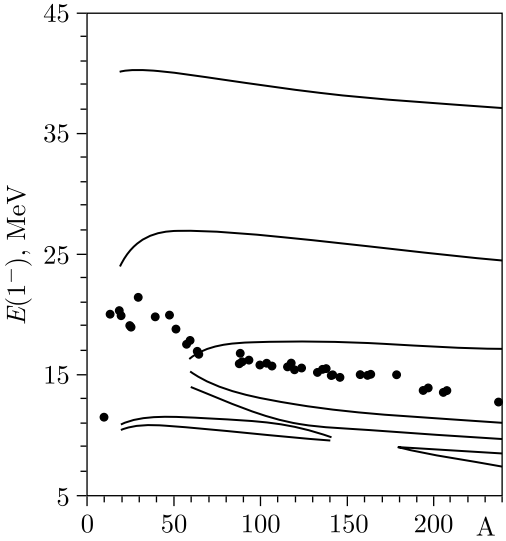

Figure 1. Energies of 1^- excitations as a function of the mass number calculated within the WFM method with SkM* force for nuclei on the beta-stability line. The solid points correspond to experimental GDR centroids. The two highest lines represent isoscalar and isovector compressional resonances. Next down, two lines are two branches of the GDR. The third from below line represents the toroidal mode. The two lowest lines can apparently be interpreted as isoscalar and isovector branches of the pygmy resonance. Reproduced from Ref. [17].

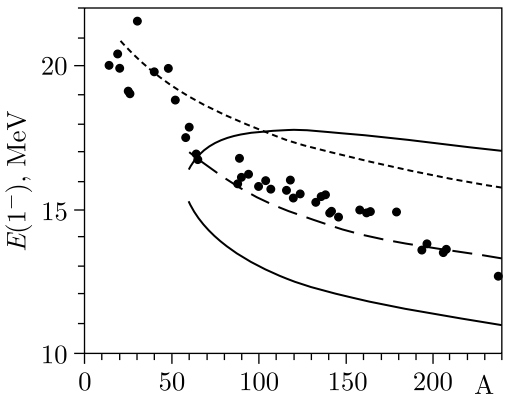

Figure 2. The 1^- excitations in the GDR (solid lines) energy region. Calculations take into account the moments of the first and third ranks. The dashed line indicates the energy centroid. The dotted line shows the results of calculations taking into account only first-rank tensors. Reproduced from Ref. [17].

Now we are going to perform calculations taking into account spin degrees of freedom and deformation. The present study is limited by moments of the first rank. Instead of Skyrme forces the harmonic oscillator with the spin-orbit potential plus separable dipole–dipole, quadrupole–quadrupole and spin-dipole–spin-dipole interactions will be used. The results of calculations for spherical nuclei are reported in Ref. [20]. We now present an extension of the theory to include deformed nuclei.

In Section 2 we briefly describe the formalism of the WFM method. The TDHF equations for density matrix are formulated, the model Hamiltonian is presented, and collective variables are defined. The derivation of the corresponding dynamical equations is discussed. Section 3 presents the results of calculations. First, the WFM equations are solved without spin-orbit potential. The ways to avoid the excitation of the center-of-mass motion are discussed. Further, the exact dynamical equations are introduced and solved. Electric $K^\pi = 0^-, 1^-$ and magnetic $K^\pi = 0^-, 1^-, 2^-$ excitations of ^{164}Dy with corresponding $E1$ and $M2$ strengths are analyzed. The origin and features of the electric spin dipole resonance are studied. The main results are reviewed and discussed in Section 4, and conclusions are given in Section 5. The mathematical details are presented in Appendix A, Appendix B, and Appendix C.

2. TDHF equation and WFM equations of motion

The TDHF equation reads [21, 22]

$$i\hbar\dot{\hat{\rho}} = \hat{h}\hat{\rho} - \hat{\rho}\hat{h}. \tag{1}$$

Let us consider its matrix form in coordinate space keeping all spin indices s, s': $\langle \mathbf{r}, s|\hat{\rho}|\mathbf{r}', s'\rangle$, etc. We do not specify the isospin indices in order to make formulae more transparent. After introduction of the more compact notation $\langle \mathbf{r}, s|\hat{X}|\mathbf{r}', s'\rangle = X^{ss'}_{rr'}$, the set of equations (1) with specified spin indices reads

$$\begin{aligned}
i\hbar\dot{\rho}^{\uparrow\uparrow}_{rr''} &= \int d^3r' \left(h^{\uparrow\uparrow}_{rr'}\rho^{\uparrow\uparrow}_{r'r''} - \rho^{\uparrow\uparrow}_{rr'}h^{\uparrow\uparrow}_{r'r''} + \hat{h}^{\uparrow\downarrow}_{rr'}\rho^{\downarrow\uparrow}_{r'r''} - \rho^{\uparrow\downarrow}_{rr'}h^{\downarrow\uparrow}_{r'r''} \right), \\
i\hbar\dot{\rho}^{\uparrow\downarrow}_{rr''} &= \int d^3r' \left(h^{\uparrow\uparrow}_{rr'}\rho^{\uparrow\downarrow}_{r'r''} - \rho^{\uparrow\uparrow}_{rr'}h^{\uparrow\downarrow}_{r'r''} + \hat{h}^{\uparrow\downarrow}_{rr'}\rho^{\downarrow\downarrow}_{r'r''} - \rho^{\uparrow\downarrow}_{rr'}h^{\downarrow\downarrow}_{r'r''} \right), \\
i\hbar\dot{\rho}^{\downarrow\uparrow}_{rr''} &= \int d^3r' \left(h^{\downarrow\uparrow}_{rr'}\rho^{\uparrow\uparrow}_{r'r''} - \rho^{\downarrow\uparrow}_{rr'}h^{\uparrow\uparrow}_{r'r''} + \hat{h}^{\downarrow\downarrow}_{rr'}\rho^{\downarrow\uparrow}_{r'r''} - \rho^{\downarrow\downarrow}_{rr'}h^{\downarrow\uparrow}_{r'r''} \right), \\
i\hbar\dot{\rho}^{\downarrow\downarrow}_{rr''} &= \int d^3r' \left(h^{\downarrow\uparrow}_{rr'}\rho^{\uparrow\downarrow}_{r'r''} - \rho^{\downarrow\uparrow}_{rr'}h^{\uparrow\downarrow}_{r'r''} + \hat{h}^{\downarrow\downarrow}_{rr'}\rho^{\downarrow\downarrow}_{r'r''} - \rho^{\downarrow\downarrow}_{rr'}h^{\downarrow\downarrow}_{r'r''} \right),
\end{aligned} \tag{2}$$

with the conventional notations $\uparrow$ for $s = 1/2$ and $\downarrow$ for $s = -1/2$.

We will consider the Wigner transform [21] of equations (2) (see Ref. [23] for mathematical details). So, instead of four (in s, s') matrix elements of the density matrix $\rho^{ss'}_{rr'}$ we will work with four Wigner functions $f^{ss'}(\mathbf{r}, \mathbf{p})$, which is more convenient for the WFM method (see Refs. [4–7]). From now on, we will not write out the coordinate dependence $(\mathbf{r}, \mathbf{p})$ of all functions in order to make formulae more transparent. We have

$$\begin{aligned}
i\hbar\dot{f}^{+} &= \frac{i\hbar}{2}\{h^{+}, f^{+}\} + \frac{i\hbar}{2}\{h^{-}, f^{-}\} + i\hbar\{h^{\uparrow\downarrow}, f^{\downarrow\uparrow}\} + i\hbar\{h^{\downarrow\uparrow}, f^{\uparrow\downarrow}\} + ..., \\
i\hbar\dot{f}^{-} &= \frac{i\hbar}{2}\{h^{+}, f^{-}\} + \frac{i\hbar}{2}\{h^{-}, f^{+}\} - 2h^{\downarrow\uparrow}f^{\uparrow\downarrow} + 2h^{\uparrow\downarrow}f^{\downarrow\uparrow} + \frac{\hbar^2}{4}\{\{h^{\downarrow\uparrow}, f^{\uparrow\downarrow}\}\} - \frac{\hbar^2}{4}\{\{h^{\uparrow\downarrow}, f^{\downarrow\uparrow}\}\} + ..., \\
i\hbar\dot{f}^{\uparrow\downarrow} &= f^{\uparrow\downarrow}h^{-} + \frac{i\hbar}{2}\{h^{+}, f^{\uparrow\downarrow}\} - \frac{\hbar^2}{8}\{\{h^{-}, f^{\uparrow\downarrow}\}\} - h^{\uparrow\downarrow}f^{-} + \frac{i\hbar}{2}\{h^{\uparrow\downarrow}, f^{+}\} + \frac{\hbar^2}{8}\{\{h^{\uparrow\downarrow}, f^{-}\}\} + ..., \\
i\hbar\dot{f}^{\downarrow\uparrow} &= -f^{\downarrow\uparrow}h^{-} + \frac{i\hbar}{2}\{h^{+}, f^{\downarrow\uparrow}\} + \frac{\hbar^2}{8}\{\{h^{-}, f^{\downarrow\uparrow}\}\} + h^{\downarrow\uparrow}f^{-} + \frac{i\hbar}{2}\{h^{\downarrow\uparrow}, f^{+}\} - \frac{\hbar^2}{8}\{\{h^{\downarrow\uparrow}, f^{-}\}\} + ...,
\end{aligned} \tag{3}$$

where the functions $h^{s,s'}$, $f^{s,s'}$ are the Wigner transforms of $h^{s,s'}_{r,r'}$, $\rho^{s,s'}_{r,r'}$, respectively; $\{f, g\}$ is the Poisson bracket of the functions f and g; $\{\{f, g\}\}$ is their double Poisson bracket;

$f^{\pm} = f^{\uparrow\uparrow} \pm f^{\downarrow\downarrow}$, and $h^{\pm} = h^{\uparrow\uparrow} \pm h^{\downarrow\downarrow}$. The dots stand for terms proportional to higher powers of $\hbar$ — after integration over phase space these terms disappear and we arrive at the set of exact integral equations.

The microscopic Hamiltonian of the model, harmonic oscillator with spin-orbit potential plus separable dipole–dipole, quadrupole–quadrupole and spin-dipole–spin-dipole interactions, is given by

$$H = \sum_{i=1}^{A} \left[\frac{\hat{\mathbf{p}}_i^2}{2m} + \frac{1}{2} m\omega^2 \mathbf{r}_i^2 - \eta \hat{\mathbf{l}}_i \hat{\mathbf{S}}_i \right] + H_{\rm dd} + H_{\rm qq} + H_{\rm sd}, \tag{4}$$

with

$$H_{\rm dd} = \sum_{\mu=-1}^{1} (-1)^{\mu} \left\{ \bar{\xi} \sum_{i}^{Z} \sum_{j}^{N} + \frac{\xi}{2} \left[\sum_{i,j(i\neq j)}^{Z} + \sum_{i,j(i\neq j)}^{N} \right] \right\} r_{-\mu}(i) r_{\mu}(j), \tag{5}$$

$$H_{\rm qq} = \sum_{\mu=-2}^{2} (-1)^{\mu} \left\{ \bar{\kappa} \sum_{i}^{Z} \sum_{j}^{N} + \frac{\kappa}{2} \left[\sum_{i,j(i\neq j)}^{Z} + \sum_{i,j(i\neq j)}^{N} \right] \right\} q_{2-\mu}(\mathbf{r}_i) q_{2\mu}(\mathbf{r}_j), \tag{6}$$

$$H_{\rm sd} = \sum_{\lambda=0}^{2} \sum_{\mu=-\lambda}^{\lambda} (-1)^{\mu} \left\{ \bar{\chi} \sum_{i}^{Z} \sum_{j}^{N} + \frac{\chi}{2} \left[\sum_{i,j(i\neq j)}^{Z} + \sum_{i,j(i\neq j)}^{N} \right] \right\} s_{\lambda-\mu}(i) s_{\lambda\mu}(j), \tag{7}$$

where $q_{2\mu}(\mathbf{r}) = \sqrt{16\pi/5}\, r^2 Y_{2\mu}(\theta,\phi) = \sqrt{6}\{r \otimes r\}_{2\mu}$, $\{r \otimes r\}_{\lambda\mu} = \sum_{\sigma,\nu} C^{\lambda\mu}_{1\sigma,1\nu} r_\sigma r_\nu$, $C^{\lambda\mu}_{1\sigma,1\nu}$ is the Clebsch–Gordan coefficient, and cyclic coordinates r_μ are defined as $r_\mu = \sqrt{4\pi/3}\, r Y_{1\mu}(\theta,\phi)$ [24]. N and Z are the numbers of neutrons and protons, $A = N+Z$, $\xi, \bar{\xi}, \kappa, \bar{\kappa}, \chi, \bar{\chi}$ and η are strength constants, $s_{\lambda\mu}$ is the spin-dipole operator [13] which is given as

$$s_{\lambda\mu} = \{\hat{S} \otimes \hat{r}\}_{\lambda\mu}/\hbar, \tag{8}$$

$\hat{S}_\mu$ are spin matrices [24]:

$$\hat{S}_1 = -\frac{\hbar}{\sqrt{2}} \begin{pmatrix} 0 & 1 \\ 0 & 0 \end{pmatrix}, \quad \hat{S}_0 = \frac{\hbar}{2} \begin{pmatrix} 1 & 0 \\ 0 & -1 \end{pmatrix}, \quad \hat{S}_{-1} = \frac{\hbar}{\sqrt{2}} \begin{pmatrix} 0 & 0 \\ 1 & 0 \end{pmatrix}.$$

The mean field generated by $H_{\rm qq}$ was processed in Ref. [4]. The mean fields generated by $H_{\rm dd}$ and $H_{\rm sd}$ are derived, and the results are written out in Appendix A.

Equations (3) will be solved in a small amplitude approximation by the WFM method. Integrating (3) over phase space with the weights r_μ and p_μ, one gets dynamical equations for the following collective variables:

$$R_\mu^{\tau\zeta}(t) = (2\pi\hbar)^{-3} \int d\mathbf{r} \int d\mathbf{p}\, r_\mu f^{\tau\zeta}(\mathbf{r},\mathbf{p},t),$$

$$P_\mu^{\tau\zeta}(t) = (2\pi\hbar)^{-3} \int d\mathbf{r} \int d\mathbf{p}\, p_\mu f^{\tau\zeta}(\mathbf{r},\mathbf{p},t), \tag{9}$$

where τ denotes the isospin index, $\zeta = +, -, \uparrow\downarrow, \downarrow\uparrow$ denotes the spin index: $+$ is spin-scalar (SS), $-$ is spin-vector (SV), and $\uparrow\downarrow$, $\downarrow\uparrow$ are spin-flip (SF).

The integration yields the sets of coupled (due to neutron–proton interaction) equations for neutron and proton variables. The found equations are nonliner due to dipole–dipole, quadrupole–quadrupole and spin-dipole–spin-dipole interactions. The small amplitude approximation allows one to linearize the equations. Writing all variables (9) as a sum of their equilibrium value (eq) plus a small deviation

$$R_\mu^{\tau\zeta}(t) = R_\mu^{\tau\zeta}(\mathrm{eq}) + \mathcal{R}_\mu^{\tau\zeta}(t), \quad P_\mu^{\tau\zeta}(t) = P_\mu^{\tau\zeta}(\mathrm{eq}) + \mathcal{P}_\mu^{\tau\zeta}(t), \tag{10}$$

with

$$\mathcal{R}_\mu^{\tau\zeta}(t) = (2\pi\hbar)^{-3}\int d\mathbf{r}\int d\mathbf{p}\, r_\mu \delta f^{\tau\zeta}(\mathbf{r},\mathbf{p},t),$$
$$\mathcal{P}_\mu^{\tau\zeta}(t) = (2\pi\hbar)^{-3}\int d\mathbf{r}\int d\mathbf{p}\, p_\mu \delta f^{\tau\zeta}(\mathbf{r},\mathbf{p},t),$$

where $\delta f^{\tau\zeta}$ is a variation of $f^{\tau\zeta}$, and neglecting quadratic deviations, one obtains the linearized equations. It is convenient to rewrite them in terms of isovector (IV) $\bar{\mathcal{R}}_\mu = \mathcal{R}_\mu^{\mathrm{n}} - \mathcal{R}_\mu^{\mathrm{p}}$, $\bar{\mathcal{P}}_\mu = \mathcal{P}_\mu^{\mathrm{n}} - \mathcal{P}_\mu^{\mathrm{p}}$ and isoscalar (IS) $\mathcal{R}_\mu = \mathcal{R}_\mu^{\mathrm{n}} + \mathcal{R}_\mu^{\mathrm{p}}$, $\mathcal{P}_\mu = \mathcal{P}_\mu^{\mathrm{n}} + \mathcal{P}_\mu^{\mathrm{p}}$ variables. We also define isovector and isoscalar quadrupole strength constants $\kappa_1 = \frac{1}{2}(\kappa - \bar{\kappa})$ and $\kappa_0 = \frac{1}{2}(\kappa + \bar{\kappa})$ connected by the relation $\kappa_1 = \alpha\kappa_0$ with $\alpha = -2$ [1]. In a similar way we introduce isovector and isoscalar dipole $\xi_1 = \frac{1}{2}(\xi - \bar{\xi})$, $\xi_0 = \frac{1}{2}(\xi + \bar{\xi})$ and spin-dipole $\chi_1 = \frac{1}{2}(\chi - \bar{\chi})$, $\chi_0 = \frac{1}{2}(\chi + \bar{\chi})$ strength constants. The complete set of dynamical equations is written out in Appendix B.

3. Results of calculations

First of all, it is necessary to determine the values of the dipole–dipole interaction constants. The most natural way is to reproduce the main characteristics of the GDR, which is one of the fundamental collective excitation modes in nuclei. The experimental position of the GDR energy centroid in medium and heavy nuclei can be fairly reproduced by the simple formula, $E(\mathrm{GDR}) \simeq 80A^{-1/3}$ MeV [21]. It is natural to fix the isovector constant ξ_1 in such a way that the theory reproduces the observed excitation energy of the GDR. The fulfillment of this requirement in the collective model developed by Bohr and Mottelson leads to $\xi_1 = \xi_{\mathrm{BM}} = 113A^{-5/3}$ MeV $\cdot$ fm^{-2} [25]. The isoscalar constant ξ_0 must be chosen so as to avoid excitation of the Center-of-Mass Motion (CMM). To this end, ξ_0 will be determined from the equation of motion for the center of mass of a nucleus. Following this procedure, we avoid the admixture of $E1$ spurious state.

The quadrupole strength constant κ_0 was determined in Ref. [2] following the condition of self-consistency between the mean field and the density [25]. The choice of spin-dipole strength constants χ_1 and χ_0 will be discussed in Subsection 3.2.

First, let's consider the simplified version of the problem, without the spin-orbit potential ($\eta = 0$). In this case, the orbital and spin degrees of freedom are separated. Such a simple model allows us to obtain analytical expressions for the energy and excitation probability of the GDR. Comparing them with the results of precise calculations, we will estimate the role of spin degrees of freedom.

Further we will analyze the magnetic excitations arising due to spin degrees of freedom.

3.1. The Giant Dipole Resonance ($\eta = 0$ limit)

3.1.1. GDR ($K^\pi = 1^-$)

The $K^\pi = 1^-$ excitations are described by system of dynamic equations (B.2) (see Appendix B). In the absence of the spin-orbit potential, this system splits into three independent

subsystems. The subsystems related to spin dynamics will be discussed later. The subsystem

$$\begin{aligned}
\dot{\bar{\mathcal{R}}}_1^+ &= \frac{1}{m}\bar{\mathcal{P}}_1^+, \\
\dot{\bar{\mathcal{P}}}_1^+ &= -m\tilde{\omega}^2\left(1+\frac{4}{3}\delta\right)\bar{\mathcal{R}}_1^+ - \frac{2}{3}\alpha\delta X m\tilde{\omega}^2\mathcal{R}_1^+ - A\left(\xi_1^{K=1}\bar{\mathcal{R}}_1^+ + X\xi_0^{K=1}\mathcal{R}_1^+\right), \\
\dot{\mathcal{R}}_1^+ &= \frac{1}{m}\mathcal{P}_1^+, \\
\dot{\mathcal{P}}_1^+ &= -m\tilde{\omega}^2\left(1+\frac{4}{3}\delta\right)\mathcal{R}_1^+ - \frac{2}{3}\alpha\delta X m\tilde{\omega}^2\bar{\mathcal{R}}_1^+ - A\left(\xi_0^{K=1}\mathcal{R}_1^+ + X\xi_1^{K=1}\bar{\mathcal{R}}_1^+\right)
\end{aligned} \tag{11}$$

describes the coupled dynamics of spin-scalar variables $\bar{\mathcal{R}}_1^+$, $\bar{\mathcal{P}}_1^+$, $\mathcal{R}_1^+$, and $\mathcal{P}_1^+$. Here δ is the deformation parameter, and $\tilde{\omega}^2 = \omega^2/(1+\frac{2}{3}\delta)$. The isoscalar variables $\mathcal{R}_1^+$ and $\mathcal{P}_1^+$ represent the displacement of the center of mass and the nucleus momentum variation, respectively. Isovector variables $\bar{\mathcal{R}}_1^+$, $\bar{\mathcal{P}}_1^+$ describe the out-of-phase translational motion of protons and neutrons (i.e., isovector GDR). Imposing the time evolution via $e^{i\Omega t}$ for all variables, one transforms (11) into a set of algebraic equations. Eigenfrequencies $\Omega^{K=1}$ are found as the solutions of its secular equation:

$$\begin{aligned}
\left[\Omega_\pm^{K=1}\right]^2 &= \tilde{\omega}^2\left(1+\frac{4}{3}\delta\right) + \frac{A}{2m}\left(\xi_0^{K=1}+\xi_1^{K=1}\right) \\
&\pm \frac{1}{2m}\sqrt{A^2\left(\xi_0^{K=1}-\xi_1^{K=1}\right)^2 + 4\left(A\xi_0^{K=1}+\frac{2}{3}\delta\alpha m\tilde{\omega}^2\right)\left(A\xi_1^{K=1}+\frac{2}{3}\delta\alpha m\tilde{\omega}^2\right)X^2}.
\end{aligned} \tag{12}$$

Here $X = (N-Z)/A$ is the asymmetry parameter. For the rest notations, see Appendix B.

The nucleus translation, i.e., CMM, should be decoupled from the physical excitations. To ensure this, the isoscalar constant $\xi_0^{K=1}$ is fixed by the condition $\Omega_{\rm IS}^{K=1} \equiv \Omega_+^{K=1} = 0$. We denote this value by $\tilde{\xi}_0^{K=1}$. From Eq. (12) we find

$$\tilde{\xi}_0^{K=1} = -\frac{m\omega^2}{A}\frac{\left(A\xi_1^{K=1}+m\omega^2C_1\right)C_1 - \frac{2}{3}\alpha\delta\tilde{\omega}^2/\omega^2\left(A\xi_1^{K=1}+\frac{2}{3}\alpha\delta m\tilde{\omega}^2\right)X^2}{A\xi_1^{K=1}+m\omega^2C_1 - X^2\left(A\xi_1^{K=1}+\frac{2}{3}\alpha\delta m\tilde{\omega}^2\right)}, \tag{13}$$

where the notation $C_1 = \left(1+\frac{4}{3}\delta\right)/\left(1+\frac{2}{3}\delta\right)$ is introduced.

For further analysis, it is useful to consider the version of calculations without coupling between isovector (IV) and isoscalar (IS) systems. To do this, it is enough to put $X = 0$. Separated equations help to classify the obtained solutions. In this case, formulas (12) and (13) take a particularly simple form:

$$\left[\Omega_{\rm IS}^{K=1}\right]^2 \equiv \left[\Omega_+^{K=1}\right]^2 = \tilde{\omega}^2\left(1+\frac{4}{3}\delta\right) + \frac{A}{m}\xi_0^{K=1}, \tag{14}$$

$$\left[\Omega_{\rm IV}^{K=1}\right]^2 \equiv \left[\Omega_-^{K=1}\right]^2 = \tilde{\omega}^2\left(1+\frac{4}{3}\delta\right) + \frac{A}{m}\xi_1^{K=1}, \tag{15}$$

$$\tilde{\xi}_0^{K=1} = -\frac{m}{A}\omega^2C_1. \tag{16}$$

The same deformation dependence is supposed for the isovector constant:

$$\xi_1^{K=1} = \xi_{\rm BM}C_1, \tag{17}$$

where $\xi_{\rm BM} = 113A^{-5/3}$ is taken from Ref. [25]. The numerical estimates in the present work will be given on the example of the nucleus ^{164}Dy with the deformation parameter $\delta = 0.26$. The values of constants are

$$\tilde{\xi}_0^{K=1} = -0.0126 \ \ \text{MeV}\cdot\text{fm}^{-2}, \quad \xi_1^{K=1} = 0.0264 \ \ \text{MeV}\cdot\text{fm}^{-2}, \tag{18}$$

and $\xi_{\rm BM} = 0.0230 \ \ \text{MeV}\cdot\text{fm}^{-2}$. The numerical value of the isoscalar constant given by formula (13) is $\tilde{\xi}_0^{K=1} = -0.0130 \ \ \text{MeV}\cdot\text{fm}^{-2}$. The comparison of this value with (18) shows that the influence of isovector–isoscalar coupling is small.

Excitation probabilities are calculated with the help of the theory of a linear response of a system to a weak external field (see Appendix C). The reduced probability for an electric dipole transition reads

$$B(E11)_\pm = \pm e^2 \frac{3\hbar}{4\pi}\frac{NZ}{A} \times \\ \times \frac{m\left(\left[\Omega_\pm^{K=1}\right]^2 - \omega^2 C_1\right) - A\xi_0^{K=1} - \left(A\xi_1^{K=1} + \frac{2}{3}\delta\alpha m\tilde{\omega}^2\right)X^2}{m\Omega_\pm^{K=1}\sqrt{A^2\left(\xi_0^{K=1} - \xi_1^{K=1}\right)^2 + 4\left(A\xi_0^{K=1} + \frac{2}{3}\delta\alpha m\tilde{\omega}^2\right)\left(A\xi_1^{K=1} + \frac{2}{3}\delta\alpha m\tilde{\omega}^2\right)X^2}}. \tag{19}$$

Neglecting here the isovector–isoscalar coupling and using (16) and (15), we easily obtain

$$B(E11)_{\rm IS} \equiv B(E11)_+ = 0, \tag{20}$$

$$B(E11)_{\rm IV} \equiv B(E11)_- = \frac{3}{4\pi}\frac{NZ}{A}\frac{e^2\hbar}{m\Omega_{\rm IV}^{K=1}}. \tag{21}$$

The results of calculations for ^{164}Dy are presented in Table 1, where the energies $E_{11} = \hbar\Omega^{K=1}$ of 1^- levels with their electric dipole strengths are shown. The left panel presents the results of calculations with the isovector–isoscalar coupling, the right panel shows the solutions of decoupled ($X = 0$) equations. From the comparison of the left and right panels, it is clear that the coupling has a minor effect on the energy and excitation probability of the GDR.

Table 1. The results of WFM calculations for ^{164}Dy without spin-orbit potential ($\eta = 0$ limit): energies E_{11} and $B(E11)$ strengths of 1^- excitations. The factor 2, which appears due to the degeneration in the sign of K, is taken into account for the $E1$ strength.

Coupled			Decoupled		
E_{11}, MeV	$B(E11)\uparrow$, e^2fm^2		E_{11}, MeV	$B(E11)\uparrow$, e^2fm^2	
		$\xi_0^{K=1}/\tilde{\xi}_0^{K=1} = 1$			
0.00	–		0.00	0.00	IS
16.28	23.86		16.35	24.07	IV
		$\xi_0^{K=1}/\tilde{\xi}_0^{K=1} = -30$			
52.56	0.00		51.78	0.00	IS
16.16	24.36		16.35	24.07	IV

In the above calculations, we excluded the excitation of the CMM by the special choice of the isoscalar constant $\xi_0^{K=1} = \tilde{\xi}_0^{K=1}$ (see Eq. (16)). However, there is one more possibility to avoid the appearance of the spurious mode. It turns out that the excitation probability of the CMM quickly decreases with the increase in the absolute value of $\xi_0^{K=1}$, the GDR energy being

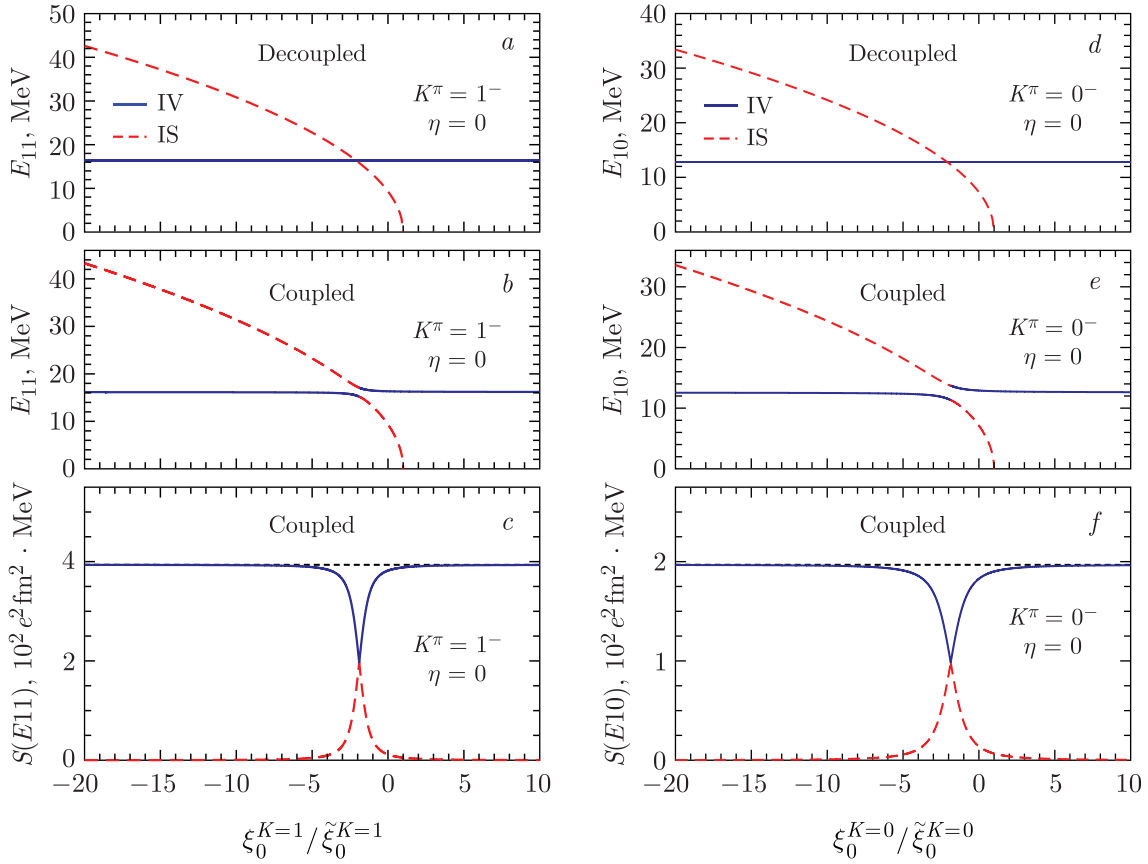

Figure 3. Energies E_{1K} (a, b, d, e) and values of $S(E1K) = E_{1K}B(E1K)$ (c, f) vs. $\xi_0^{K=\mu}/\tilde{\xi}_0^{K=\mu}$ ratio. The calculations are performed for ^{164}Dy without the spin-orbit interaction ($\eta = 0$). The solid blue line corresponds to the GDR, and the dashed red line to the CMM. The black short dashed lines in the panels (c) and (f) indicate the EWSR (33) values.

practically unchanged. This situation is also demonstrated by Table 1, where the results of calculations for two different values of $\xi_0^{K=1}$ are compared. In the case of $\xi_0^{K=1} = \tilde{\xi}_0^{K=1}$, the CMM energy E_{CM} and the corresponding $E1$ strength are equal to zero (see the first line in Table 1), whereas the GDR energy and its $B(E11)$ have their standard values. In the case of $\xi_0^{K=1} = -30\tilde{\xi}_0^{K=1}$, the energy E_{CM} increase to 52.56 MeV with $B(E11) \simeq 0$, the changes in the GDR characteristics being very small. The energies E_{11} of the GDR and CMM as the functions of the ratio $\xi_0^{K=1}/\tilde{\xi}_0^{K=1}$ are shown in Figure 3 for $X = 0$ (a) and $X \neq 0$ (b). One can see that the coupling has little influence on the overall picture of the energy behaviour.

3.1.2. GDR ($K^\pi = 0^-$)

The $K^\pi = 0^-$ excitations are described by the system of dynamic equations (B.3) (see Appendix B). In the $\eta = 0$ limit, this system splits. The system for spin-independent variables reads

$$\begin{aligned}
\dot{\bar{\mathcal{R}}}_0^+ &= \frac{1}{m}\bar{\mathcal{P}}_0^+, \\
\dot{\bar{\mathcal{P}}}_0^+ &= -m\tilde{\omega}^2\left(1 - \frac{2}{3}\delta\right)\bar{\mathcal{R}}_0^+ + \frac{4}{3}\alpha\delta X m\tilde{\omega}^2\mathcal{R}_0^+ - A\left(\xi_1^{K=0}\bar{\mathcal{R}}_0^+ + X\xi_0^{K=0}\mathcal{R}_0^+\right), \\
\dot{\mathcal{R}}_0^+ &= \frac{1}{m}\mathcal{P}_0^+, \\
\dot{\mathcal{P}}_0^+ &= -m\tilde{\omega}^2\left(1 - \frac{2}{3}\delta\right)\mathcal{R}_0^+ + \frac{4}{3}\alpha\delta X m\tilde{\omega}^2\bar{\mathcal{R}}_0^+ - A\left(\xi_0^{K=0}\mathcal{R}_0^+ + X\xi_1^{K=0}\bar{\mathcal{R}}_0^+\right).
\end{aligned} \tag{22}$$

The characteristic equation of the respective set of algebraic equations has two eigenvalues

$$\left[\Omega_{\pm}^{K=0}\right]^2 = \tilde{\omega}^2\left(1-\frac{2}{3}\delta\right)+\frac{A}{2m}\left(\xi_0^{K=0}+\xi_1^{K=0}\right) \pm \frac{1}{2m}\sqrt{A^2\left(\xi_0^{K=0}-\xi_1^{K=0}\right)^2+4\left(A\xi_0^{K=0}-\frac{4}{3}\delta\alpha m\tilde{\omega}^2\right)\left(A\xi_1^{K=0}-\frac{4}{3}\delta\alpha m\tilde{\omega}^2\right)X^2}. \quad (23)$$

Without isovector–isoscalar coupling ($X=0$), they are simplified to

$$\left[\Omega_{\rm IS}^{K=0}\right]^2 \equiv \left[\Omega_{+}^{K=0}\right]^2 = \tilde{\omega}^2\left(1-\frac{2}{3}\delta\right)+\frac{A}{m}\xi_0^{K=0}, \quad (24)$$

$$\left[\Omega_{\rm IV}^{K=0}\right]^2 \equiv \left[\Omega_{-}^{K=0}\right]^2 = \tilde{\omega}^2\left(1-\frac{2}{3}\delta\right)+\frac{A}{m}\xi_1^{K=0}. \quad (25)$$

Analogously to the case of $K^\pi=1^-$, we find from the condition $\Omega_{\rm IS}^{K=0}=0$ that

$$\tilde{\xi}_0^{K=0} = -\frac{m}{A}\omega^2 C_0, \quad (26)$$

where $C_0 = \left(1-\frac{2}{3}\delta\right)/\left(1+\frac{2}{3}\delta\right)$. For the isovector constant in (25), we take

$$\xi_1^{K=0} = \xi_{\rm BM} C_0, \quad (27)$$

Numerical values of these constants for ^{164}Dy are

$$\tilde{\xi}_0^{K=0} = -0.0077 \ \ \text{MeV}\cdot\text{fm}^{-2}, \quad \xi_1^{K=0} = 0.0162 \ \ \text{MeV}\cdot\text{fm}^{-2}. \quad (28)$$

In general case ($X\neq 0$), the condition $\Omega_{+}^{K=0}=0$ is satisfied by

$$\tilde{\xi}_0^{K=0} = -\frac{m}{A}\frac{\left(A\xi_1^{K=0}+m\omega^2C_0\right)\omega^2C_0+\frac{4}{3}\alpha\delta\tilde{\omega}^2\left(A\xi_1^{K=0}-\frac{4}{3}\alpha\delta m\tilde{\omega}^2\right)X^2}{A\xi_1^{K=0}+m\omega^2C_0-X^2\left(A\xi_1^{K=0}-\frac{4}{3}\alpha\delta m\tilde{\omega}^2\right)}. \quad (29)$$

For ^{164}Dy Eq. (29) gives $\tilde{\xi}_0^{K=0} = -0.0078 \ \ \text{MeV}\cdot\text{fm}^{-2}$; i.e., the influence of isovector–isoscalar coupling on the value of the $\tilde{\xi}_0^{K=0}$ is very small (exactly as in the case of $K^\pi=1^-$). The excitation probability is calculated in the same way as for $K^\pi=1^-$. The $B(E10)$ strength reads

$$B(E10)_{\pm} = \pm e^2\frac{3\hbar}{4\pi}\frac{NZ}{A}\times \times \frac{m\left(\left[\Omega_{\pm}^{K=0}\right]^2-\omega^2C_0\right)-A\xi_0^{K=0}-\left(A\xi_1^{K=0}-\frac{4}{3}\delta\alpha m\tilde{\omega}^2\right)X^2}{m\Omega_{\pm}^{K=0}\sqrt{A^2\left(\xi_0^{K=0}-\xi_1^{K=0}\right)^2+4\left(A\xi_0^{K=0}-\frac{4}{3}\delta\alpha m\tilde{\omega}^2\right)\left(A\xi_1^{K=0}-\frac{4}{3}\delta\alpha m\tilde{\omega}^2\right)X^2}}. \quad (30)$$

Neglecting the terms proportional to X, one gets

$$B(E10)_{\rm IS} \equiv B(E10)_{+} = 0, \quad (31)$$

$$B(E10)_{\rm IV} \equiv B(E10)_{-} = \frac{3}{4\pi}\frac{NZ}{A}\frac{e^2\hbar}{2m\Omega_{\rm IV}^{K=0}}. \quad (32)$$

The results of calculations for ^{164}Dy are presented in Table 2. We again have considered various scenarios for eliminating CMM excitation. The results are given for two different values of $\xi_0^{K=0}$. The energies E_{10} of the GDR and CMM excitations as functions of $\xi_0^{K=0}/\tilde{\xi}_0^{K=0}$ are shown in Figure 3 for $X=0$ (d) and $X\neq 0$ (e). The influence of the isovector–isoscalar coupling is insignificant analogously to the case of $K^\pi=1^-$.

Table 2. The results of WFM calculations for ^{164}Dy without spin-orbit potential ($\eta = 0$ limit): energies E_{10} and $B(E10)$ strengths.

Coupled			Decoupled		
E_{10}, MeV	$B(E10)$, e^2fm^2		E_{10}, MeV	$B(E10)$, e^2fm^2	
		$\xi_0^{K=0}/\tilde{\xi}_0^{K=0} = 1$			
0.00	–		0.00	0.00	IS
12.80	14.85		12.81	15.36	IV
		$\xi_0^{K=0}/\tilde{\xi}_0^{K=0} = -30$			
40.76	0.00		40.57	0.00	IS
12.56	15.67		12.81	15.36	IV

3.1.3. GDR sum rule

The experimental position of the GDR energy centroid in medium and heavy nuclei follows a simple A dependence: $E_{\rm GDR} = 80A^{-1/3}$ [MeV]. In deformed axially symmetric nuclei, the GDR strength is split into two components, corresponding to oscillations of neutrons against protons along ($K = 0$) and perpendicular ($|K| = 1$) to the symmetry axis. The energy separation was found to be proportional to the ground state deformation δ: $\Delta_{\rm GDR} = E_{11} - E_{10} \simeq E_{\rm GDR}\delta$ [26]. For ^{164}Dy, the above fitting formulas produce $E_{\rm GDR} = 14.62$ MeV and $\Delta_{\rm GDR} = 3.80$ MeV. Our calculations within the WFM method lead to the energy position $E_{10} = 12.80$ (12.56) MeV and $E_{11} = 16.28$ (16.16) MeV (see Tables 1 and 2). So for the GDR centroid and splitting we find $\bar{E}_{\rm GDR} = 14.94$ (14.75) MeV and $\Delta_{\rm GDR} = 3.48$ (3.60) MeV. These values are in fairly good agreement with the empirical estimates for GDR given above.

We find that our calculations exhaust 100% of the classical energy-weighted sum rule (EWSR) [25]

$$S_1(E1, K) = \frac{3}{4\pi}\frac{\hbar^2}{2m}\frac{NZ}{A}e^2, \tag{33}$$

when the energy of the CMM is pushed to the high energy region. If the admixture of $E1$ spurious state is eliminated by zeroing the CMM excitation energy, then the exhaustion of the sum rule is 98%. The rest 2% are taken by the CMM. The results of calculations of $S(E1K) = E_{1K}B(E1K)$ in the case of $X \neq 0$ (coupled) are shown in Figures 3, c and 3, f depending on the ratio $\xi_0^K/\tilde{\xi}_0^K$ for ^{164}Dy. The black tiny dashed lines indicate the EWSR values given by Eq. (33).

Figures 3, b and 3, e demonstrate the usual quantum mechanical quasi-crossings of the energy levels. The reliable results for the GDR energy and the sum rule are obtained for all ξ_0 excluding the values in the vicinity of the quasi-crossing point.

3.2. Spin-dependent excitations ($\eta = 0$ limit)

In this paper, the study is limited by tensors of the first rank. The procedure for calculating excitation probabilities is described in Appendix C. As follows from (C.12), the orbital part of the $M2$ response is expressed through third-rank tensors (C.13). Orbital 2^- excitations were studied within the WFM method using Skyrme forces in the paper [19]. However, microscopic estimates indicate that $M2$ transitions are mainly determined by the spin response, see [16, 27, 28]. In the present consideration, the spin contribution (C.14) to $B(M2)$ will be estimated.

3.2.1. $K^\pi = 1^-$

The $K^\pi = 1^-$ excitations are described by the system of dynamic equations (B.2) (see Appendix B). In the $\eta = 0$ limit, the system (B.2) splits into three independent subsets. The one

that describes the $K^\pi = 1^-$ component of GDR (11), was analyzed above. The second subsystem describes the dynamics of SV isovector $\bar{\mathcal{R}}_1^-$, $\bar{\mathcal{P}}_1^-$ and SV isoscalar $\mathcal{R}_1^-$, $\mathcal{P}_1^-$ variables:

$$\begin{aligned}
\dot{\bar{\mathcal{R}}}_1^- &= \frac{1}{m}\bar{\mathcal{P}}_1^-, \\
\dot{\bar{\mathcal{P}}}_1^- &= -m\omega^2 C_1 \bar{\mathcal{R}}_1^- - \frac{2}{3}\alpha\delta X m\tilde{\omega}^2 \mathcal{R}_1^- - \frac{A}{4}\left(\chi_1 \bar{\mathcal{R}}_1^- + \chi_0 X \mathcal{R}_1^-\right), \\
\dot{\mathcal{R}}_1^- &= \frac{1}{m}\mathcal{P}_1^-, \\
\dot{\mathcal{P}}_1^- &= -m\omega^2 C_1 \mathcal{R}_1^- - \frac{2}{3}\alpha\delta X m\tilde{\omega}^2 \bar{\mathcal{R}}_1^- - \frac{A}{4}\left(\chi_0 \mathcal{R}_1^- + \chi_1 X \bar{\mathcal{R}}_1^-\right).
\end{aligned} \tag{34}$$

The solution of its secular equation gives

$$\left[\Omega_\pm^{K=1}\right]^2_{\rm SV} = \omega^2 C_1 + \frac{A}{8m}\left(\chi_0 + \chi_1 \pm \sqrt{\mathcal{G}_1}\right), \tag{35}$$

where

$$\mathcal{G}_1 = (\chi_0 - \chi_1)^2 + 4X^2\left[\chi_0 + \frac{8}{3A}\delta\alpha m\tilde{\omega}^2\right]\left[\chi_1 + \frac{8}{3A}\delta\alpha m\tilde{\omega}^2\right]. \tag{36}$$

The third subsystem contains only SF variables:

$$\begin{aligned}
\dot{\bar{\mathcal{R}}}_0^{\downarrow\uparrow} &= \frac{1}{m}\bar{\mathcal{P}}_0^{\downarrow\uparrow}, \\
\dot{\bar{\mathcal{P}}}_0^{\downarrow\uparrow} &= -m\omega^2 C_0 \bar{\mathcal{R}}_0^{\downarrow\uparrow} + \frac{4}{3}\alpha\delta X m\tilde{\omega}^2 \mathcal{R}_0^{\downarrow\uparrow} - \frac{A}{4}\left(\chi_1 \bar{\mathcal{R}}_0^{\downarrow\uparrow} + \chi_0 X \mathcal{R}_0^{\downarrow\uparrow}\right), \\
\dot{\mathcal{R}}_0^{\downarrow\uparrow} &= \frac{1}{m}\mathcal{P}_0^{\downarrow\uparrow}, \\
\dot{\mathcal{P}}_0^{\downarrow\uparrow} &= -m\omega^2 C_0 \mathcal{R}_0^{\downarrow\uparrow} + \frac{4}{3}\alpha\delta X m\tilde{\omega}^2 \bar{\mathcal{R}}_0^{\downarrow\uparrow} - \frac{A}{4}\left(\chi_0 \mathcal{R}_0^{\downarrow\uparrow} + \chi_1 X \bar{\mathcal{R}}_0^{\downarrow\uparrow}\right).
\end{aligned} \tag{37}$$

The corresponding eigenfrequencies are

$$\left[\Omega_\pm^{K=1}\right]^2_{\rm SF} = \omega^2 C_0 + \frac{A}{8m}\left(\chi_0 + \chi_1 \pm \sqrt{\mathcal{G}_0}\right), \tag{38}$$

with

$$\mathcal{G}_0 = (\chi_0 - \chi_1)^2 + 4X^2\left[\chi_0 - \frac{16}{3A}\delta\alpha m\tilde{\omega}^2\right]\left[\chi_1 - \frac{16}{3A}\delta\alpha m\tilde{\omega}^2\right]. \tag{39}$$

As follows from Eq. (C.19), the above variables are related to the $K^\pi = 1^-$ branch of the spin magnetic quadrupole resonance.

The energy position of the $M2$ states depends on the spin-dipole interaction constants χ_0 and χ_1. We adopt the $\chi_0 = -\dfrac{4\pi\kappa_{\rm sd}}{A\langle r^2\rangle}\dfrac{3}{4\pi}$ MeV/fm^2 with $\chi_1 = \alpha_1\chi_0$. The value $\kappa_{\rm sd} = 25$ MeV was chosen by analyzing the 2^- strength distribution in ^{208}Pb within the RPA in Ref. [14]. The results of our calculations using this value of $\kappa_{\rm sd}$ for ^{208}Pb [20] are in overall agreement with the results obtained within the RQRPA framework, see Ref. [16]. Since there are no other justified criteria for fixing the value of this constant, we adopt $\kappa_{\rm sd} = 25$ MeV for our calculations. We also take $\alpha_1 = -2$, the same as for the quadrupole–quadrupole interaction.

Table 3. The magnetic spin-vector (SV) and spin-flip (SF) $K^\pi = 1^-$ excitations of ^{164}Dy.

	Coupled		Decoupled		
	E_{21}	$B(M21)\uparrow$	E_{21}	$B(M21)\uparrow$	
SV	7.61	14.89	7.55	102.72	IS
	12.02	1766.92	12.06	1841.27	IV
SF	4.79	212.62	4.86	159.57	IS
	10.61	1916.18	10.58	2097.89	IV

The calculated energies and $B(M21)\uparrow$ values for ^{164}Dy are shown in Table 3. The quenching $q = 0.7$ of the spin gyromagnetic factor ($g_s = qg_s^{\text{free}}$) was used in the calculations of magnetic strengths, see (C.2) in Appendix C. Most of the strength is contained in the isovector excitations. The summed value of $B(M21)\uparrow$ for all four 1^- states is 3910.60 $\mu_N^2\text{fm}^2$.

The EWSR $S_1^\sigma(M2,K)$ coming from double commutator of the spin part of $\hat{O}(M2,K)$ operator (C.11) with the Hamiltonian takes the following form:

$$S^\sigma(M2,K) = \frac{15}{16\pi}\frac{\hbar^2}{m}\left[(g_s^{\text{n}})^2 N + (g_s^{\text{p}})^2 Z\right]\mu_N^2. \tag{40}$$

It is easy to check that energy-weighted summation over the states listed in Table 3 exhausts 100% of the EWSR (40).

3.2.2. $K^\pi = 0^-$

The $K^\pi = 0^-$ excitations are described by the system of dynamic equations (B.3) (see Appendix B). By the simple change of variables

$$\mathcal{R}_0^E = \mathcal{R}_1^{\uparrow\downarrow} + \mathcal{R}_{-1}^{\downarrow\uparrow}, \quad \mathcal{P}_0^E = \mathcal{P}_1^{\uparrow\downarrow} + \mathcal{P}_{-1}^{\downarrow\uparrow} \tag{41}$$

$$\mathcal{R}_0^M = \mathcal{R}_1^{\uparrow\downarrow} - \mathcal{R}_{-1}^{\downarrow\uparrow}, \quad \mathcal{P}_0^M = \mathcal{P}_1^{\uparrow\downarrow} - \mathcal{P}_{-1}^{\downarrow\uparrow}, \tag{42}$$

the system (B.3) is transformed into three independent subsystems (B.4), (B.5) and (B.6).

In the case of $\eta = 0$, the set (B.4) in its turn splits into two independent subsets. One describes the $K^\pi = 0^-$ branch of the GDR, see Eq. (22). The remaining subsystem for the variables $\mathcal{R}_0^E$, $\mathcal{P}_0^E$ reads

$$\begin{aligned}
\dot{\bar{\mathcal{R}}}_0^E &= \frac{1}{m}\bar{\mathcal{P}}_0^E, \\
\dot{\bar{\mathcal{P}}}_0^E &= -m\omega^2 C_1 \bar{\mathcal{R}}_0^E - \frac{2}{3}\alpha\delta X m\tilde{\omega}^2 \mathcal{R}_0^E - \frac{A}{4}\left(\chi_1 \bar{\mathcal{R}}_0^E + \chi_0 X \mathcal{R}_0^E\right), \\
\dot{\mathcal{R}}_0^E &= \frac{1}{m}\mathcal{P}_0^E, \\
\dot{\mathcal{P}}_0^E &= -m\omega^2 C_1 \mathcal{R}_0^E - \frac{2}{3}\alpha\delta X m\tilde{\omega}^2 \bar{\mathcal{R}}_0^E - \frac{A}{4}\left(\chi_0 \mathcal{R}_0^E + \chi_1 X \bar{\mathcal{R}}_0^E\right).
\end{aligned} \tag{43}$$

Equations (43) formally coincide with Eq. (34) — the only difference is in the notations of variables. Naturally the eigenfrequencies of both systems also coincide. The respective two states in ^{164}Dy have energies of 7.61 and 12.02 MeV. However they are not excited, because the variables $\mathcal{R}_0^E, \mathcal{P}_0^E$ are not disturbed by any of the electromagnetic operators, see Appendix C. The situation is changed in the case of $\eta \neq 0$ (see Table 4).

Table 4. The electric $K^\pi = 0^-$ excitations of ^{164}Dy.

		E_{10}, MeV	$B(E10)$, $e^2\text{fm}^2$
		$\xi_0^{K=1}/\tilde{\xi}_0^{K=1} = 1$	
IS	SS	0.00	—
IS	SF	7.69	0.05
IV	SF	11.64	3.65
IV	SS	13.19	11.17
		$\xi_0^{K=1}/\tilde{\xi}_0^{K=1} = -30$	
IS	SS	40.61	0.00
IS	SF	7.57	0.00
IV	SF	11.57	4.93
IV	SS	13.01	10.73

The sets (B.5) and (B.6) describe spin magnetic $K^\pi = 0^-$ transitions. It is necessary to emphasize that separation occurs already in the general case (i.e., for $\eta \neq 0$). Nevertheless, even in this case the sets (B.5) and (B.6) do not include η. That is why it will be analyzed in Subsubsection 3.3.1.

3.3. Exact calculations ($\eta \neq 0$)

Now we repeat the calculations, this time taking into account the spin-orbit potential. In this case, the $\tilde{\xi}_0^K$ constant of the dipole–dipole interaction reads

$$\tilde{\xi}_0^K = \frac{-\xi_1^K A\,(B_K - X^2 D_K) - B_K^2 + X^2 D_K^2}{A\,(\xi_1^K A(1-X^2) + B_K - X^2 D_K)}, \tag{44}$$

where $\xi_1^K = \xi_{\text{BM}} C_K$, $B_K = m\omega^2 C_K - \dfrac{\hbar^2}{4}\eta^2$ and $D_1 = \dfrac{2}{3} m\tilde{\omega}^2 \delta\alpha$, $D_0 = -\dfrac{4}{3} m\tilde{\omega}^2 \delta\alpha$. The constants of the spin-dipole–spin-dipole interaction χ_0 and χ_1 are the same as in the previous subsection.

The found states are of a complicated nature. However, based on the results of the previous subsection, it is possible to trace the origin of each solution. Further we will indicate the predominant contributions (IS, IV, SS, SV, SF).

3.3.1. $K^\pi = 0^-$

The characteristic equation of the set (B.4) describing $K^\pi = 0^-$ **electric** excitations has four eigenvalues. The $E10$ strength is calculated for each state. Results of calculations are shown in Table 4. As before, two methods are used to eliminate the excitation of the center-of-mass motion. The 13.19 (13.01) MeV state is the $K^\pi = 0^-$ branch of the GDR determined by the dynamics of spin-scalar variables $\bar{\mathcal{R}}_0^+$, $\bar{\mathcal{P}}_0^+$. The way that moves the CMM energies to the high energy region is more preferable, since it allows one to completely avoid the admixture of spurious (IS SS) 0^- state (see the bottom part of Table 4). In this case, all excitations in sum exhaust 100% of the dipole sum rule (33). So from now on we will follow this way.

Excitations at energies of 7.57 and 11.57 MeV are generated by the variables $\mathcal{R}_0^E$ and $\mathcal{P}_0^E$ defined by Eq. (41). It can be shown that $\mathcal{R}_0^E$ is the average value of the spin-dipole operator s_{10} (8):

$$\langle s_{10}\rangle = -\frac{i}{2\sqrt{2}}\text{Tr}\,(\hat{\rho}[\hat{\mathbf{r}}\times\hat{\sigma}]_z) = -\frac{i}{2\sqrt{2}}\langle \hat{x}\hat{\sigma}_y - \hat{y}\hat{\sigma}_x\rangle = -\frac{1}{2}\left(R_1^{\uparrow\downarrow} + R_{-1}^{\downarrow\uparrow}\right) = -\frac{1}{2}R_0^E, \tag{45}$$

where $\hat{\rho}$ is a density matrix and $\hat{\sigma}_i$ are Pauli matrices [24]. Analogously,

$$-\frac{i}{2\sqrt{2}}\mathrm{Tr}\left(\hat{\rho}[\hat{\mathbf{p}}\times\hat{\sigma}]_z\right)=-\frac{i}{2\sqrt{2}}\langle\hat{p}_x\hat{\sigma}_y-\hat{p}_y\hat{\sigma}_x\rangle=-\frac{1}{2}\left(P_1^{\uparrow\downarrow}+P_{-1}^{\downarrow\uparrow}\right)=-\frac{1}{2}P_0^E. \tag{46}$$

Expressions (45) and (46) show that electric spin-dipole excitations (oscillations along the z-axis) are caused by spin-flip transitions. The procedure used to eliminate the contribution of the CMM also depresses the isoscalar spin dipole state (compare IS SF lines in Table 4). The state with an energy of 11.57 MeV is the isovector Electric Spin Dipole Resonance (ESDR).

The energy centroid of two isovector electric excitations (GDR and ESDR), $\bar{E}_{10}=12.56$ MeV, and the sum of their excitation probabilities $\sum B(E10)=15.66\ e^2\mathrm{fm}^2$ are almost identical to those obtained for the GDR in the $\eta=0$ approximation (compare with Table 2). The ESDR is not excited when $\eta=0$ (see Subsubsection 3.2.2). The inclusion of the spin-orbit potential results in a slight change in the energy of both modes. The energy of the GDR changes from 12.56 MeV ($\eta=0$) to 13.01 MeV. At the same time, the energy of the ESDR changes from 12.02 to 11.57 MeV. Herewith, part of the $E1$ strength of the GDR is transferred to the ESDR, see Table 4. So, the inclusion of the spin-orbit potential opens the channel by which the ESDR takes away the essential part of the strength from the GDR. The gap between the GDR and the ESDR is $\Delta_{\mathrm{sd}}=E_{\mathrm{GDR}}-E_{\mathrm{ESDR}}=0.54$ MeV when $\eta=0$, and it increases to $\Delta_{\mathrm{sd}}=1.44$ MeV in exact calculations.

The dependence of the GDR and ESDR characteristics on the deformation is shown in Figure 4. As can be seen, with increasing deformation the splitting Δ_{sd} decreases, while the share of the strength attributed to the ESDR increases, its contribution to the EWSR increasing from 2.21% for $\delta=0$ to 28.98% for $\delta=0.26$. In the spherical limit, the splitting is maximal, $\Delta_{\mathrm{sd}}=3.87$ MeV, while the excitation probability is only 1.23 ($=3\cdot0.41$) $e^2\mathrm{fm}^2$. The energy centroid shifts toward lower energies from 14.40 MeV when $\delta=0$ to 12.56 MeV for $\delta=0.26$, the summed $E10$ strength increases from 13.66 to 15.66 $e^2\mathrm{fm}^2$.

The characteristic equations of the set (B.5) and the set (B.6) describe the SV and SF $K^\pi=0^-$ spin **magnetic** quadrupole responses, respectively. Consequently, the variables $\mathcal{R}_0^-, P_0^-$ (the set (B.5)) generate SV excitations, whereas the variables $\mathcal{R}_0^M, P_0^M$ (the set (B.6)) generate SF

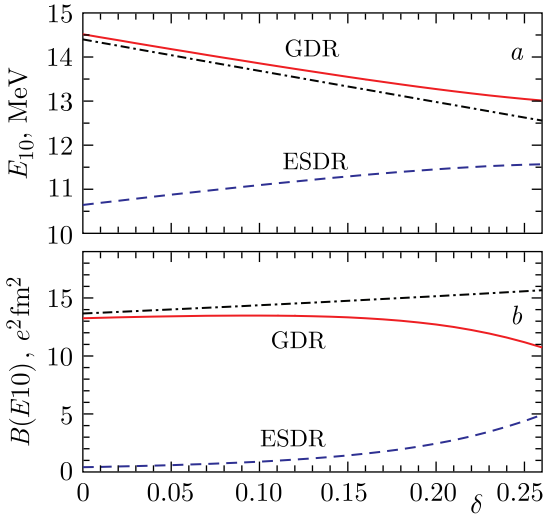

Figure 4. Energies (a) and $E1$ strengths (b) of $K^\pi=0^-$ GDR (red line) and ESDR (blue dashed line) vs. deformation δ. The energy centroid $\bar{E}_{10}$ and summed $B(E10)$ value are shown by black dot-dashed lines. Calculations are performed for ^{164}Dy.

Table 5. The magnetic $K^\pi = 0^-$ excitations of ^{164}Dy.

		E_{20}, MeV	$B(M20)$, μ_N^2fm^2
IS	SV	4.79	141.75
IV		10.61	1277.45
IS	SF	7.61	4.96
IV		12.02	588.97

excitations. Results of calculations are shown in Table 5. It can be shown that $\mathcal{R}_0^-$ and $\mathcal{R}_0^M$ are the simple combinations of average values of spin-dipole operators s_{20} and s_{00} (8):

$$\langle \hat{s}_{20} \rangle = \frac{1}{\sqrt{6}} \left[\mathcal{R}_0^- + \frac{\mathcal{R}_0^M}{\sqrt{2}} \right], \tag{47}$$

$$\langle \hat{s}_{00} \rangle = -\frac{1}{\sqrt{6}} \left[\frac{\mathcal{R}_0^-}{\sqrt{2}} - \mathcal{R}_0^M \right]. \tag{48}$$

The summed $\sum B(M20)$ strength over all four states amounts to 2013.13 μ_N^2fm^2. The magnetic EWSR (40) is completely exhausted, with 63.5% coming from a strong peak at 10.61 MeV.

3.3.2. $K^\pi = 1^-$

In deformed nuclei, the electric and magnetic channels of 1^- excitation are coupled. That is why the dynamical equations for SS variables $\bar{\mathcal{R}}_1^+$,$\bar{\mathcal{P}}_1^+$, $\mathcal{R}_1^+$, $\mathcal{P}_1^+$ and SV ($\bar{\mathcal{R}}_1^-$,$\bar{\mathcal{P}}_1^-$, $\mathcal{R}_1^-$, $\mathcal{P}_1^-$) and SF ($\bar{\mathcal{R}}_0^{\downarrow\uparrow}$,$\bar{\mathcal{P}}_0^{\downarrow\uparrow}$, $\mathcal{R}_0^{\downarrow\uparrow}$, $\mathcal{P}_0^{\downarrow\uparrow}$) variables are also coupled (see Eq. (B.2)). The characteristic equation of this system has six eigenvalues. They are shown in Table 6 together with the $B(E11)$ and $B(M21)$ reduced transition probabilities.

Table 6. The results of WFM calculations for ^{164}Dy: energies $E_{\lambda 1}$ of 1^- excitations and $B(E11)\uparrow$ and $B(M21)\uparrow$ transition probabilities. The spin-vector contributions to $B(M21)\uparrow$ ($\sim \bar{\mathcal{R}}_1^-$, $\mathcal{R}_1^-$) are indicated in brackets.

		$E_{\lambda 1}$, MeV	$B(E11)\uparrow$, e^2fm^2	$B(M21)\uparrow$, μ_N^2fm^2
			$\xi_0^{K=1}/\tilde{\xi}_0^{K=1} = 1$	
IS	SS	0.00	–	0.00
IS	SF	4.86	0.03	214.42 (0.01)
IS	SV	7.65	0.01	12.51 (14.61)
IV	SF	10.57	0.17	1793.50 (1.54)
IV	SV	11.97	0.26	1887.98 (1745.60)
IV	SS	16.37	23.42	0.92
			$\xi_0^{K=1}/\tilde{\xi}_0^{K=1} = -30$	
IS	SS	52.44	0.00	0.00
IS	SF	4.77	0.00	212.19 (0.00)
IS	SV	7.59	0.00	15.77 (15.01)
IV	SF	10.57	0.17	1794.12 (1.53)
IV	SV	11.97	0.28	1887.98 (1744.10)
IV	SS	16.25	23.90	1.08

The inclusion of the spin-orbit potential leads to the negligible increase in the GDR energy from 16.28 to 16.37 MeV (or from 16.16 to 16.25 MeV) and to the decrease of the $E1$ strength about 1% (compare the results in Table 6 with those in Table 1). That is, the GDR is weakly sensitive to a spin-orbit potential.

Zeroing the CMM excitation energy yields an exhaustion of the dipole EWSR (33) by 98.73%. The rest 1.27% are taken by the CMM. The calculations exhaust 100% of the EWSR when the energy of the CMM is pushed to the high energy region. This way wins again because it avoids the admixture of a spurious state (see IS SS in the bottom part of Table 6). The largest contribution to the EWSR, 98.68%, comes from the GDR.

The summed $M21$ strength amounts to 3911.14 $\mu_N^2\text{fm}^2$ and the magnetic EWSR (40) is exhausted by 100%. The share of the GDR is less than 1%.

The detailed analysis of the structure of magnetic 1^- excitations revealed that the SV contribution dominates in the 7.59 MeV and 11.97 MeV transitions, while the SF contribution dominates in the 4.77 MeV and 10.57 MeV transitions (see Table 6 where SV contribution to $B(M21)$ is given in brackets). The influence of the spin-orbit potential can be evaluated by comparing the results shown in Table 6 with the results of Table 3. As can be seen, the excitation energies remain almost the same. A noticeable result is that the $M21$ strength of isovector states is redistributed in favor of the SV ones.

It was shown in Subsubsection 3.3.1 that the ESDR is mediated by the operator s_{10}, which generates spin-flip transitions. For the operator s_{11} the following holds:

$$\langle s_{11}\rangle = -\frac{1}{\sqrt{2}}\left(R_1^- + \sqrt{2}R_0^{\downarrow\uparrow}\right). \tag{49}$$

Unlike $\langle s_{10}\rangle$, in addition to the spin-flip, there is also the spin-vector contribution. Herewith, the magnetic response is determined by

$$\langle s_{21}\rangle = \frac{1}{2\sqrt{2}}\left(R_1^- - \sqrt{2}R_0^{\downarrow\uparrow}\right). \tag{50}$$

Thus, in contrast with 0^-, the same variables govern both the electrical and magnetic response. Two $K^\pi = 1^-$ isovector states with energies of 10.57 and 11.97 MeV exhaust 97% of the magnetic EWSR. They also take 1.3% of the electrical EWSR. Both the spin-flip and the spin-vector oscillations contribute to the formation of these states. The analysis revealed that the spin-flip response ($\sim \bar{R}_0^{\downarrow\uparrow}$) dominates at 10.57 MeV excitation. The spin-vector vibrations ($\sim \bar{R}_1^-$) produce the dominant contribution to the 11.97 MeV excitation, see Table 6. In general, the electric spin response is suppressed by the magnetic one in electromagnetic transitions.

3.3.3. $K^\pi = 2^-$

The system of equations (B.1) describing the $K^\pi = 2^-$ component of the spin $M2$ resonance coincides with Eqs. (34), the difference being again only in the notations of variables:

$$\begin{aligned}
\dot{\bar{\mathcal{R}}}_1^{\downarrow\uparrow} &= \frac{1}{m}\bar{\mathcal{P}}_1^{\downarrow\uparrow},\\
\dot{\bar{\mathcal{P}}}_1^{\downarrow\uparrow} &= -m\omega^2 C_1\bar{\mathcal{R}}_1^{\downarrow\uparrow} - \frac{2}{3}\alpha\delta X m\tilde{\omega}^2\mathcal{R}_1^{\downarrow\uparrow} - \frac{A}{4}\left(\chi_1\bar{\mathcal{R}}_1^{\downarrow\uparrow} + \chi_0 X\mathcal{R}_1^{\downarrow\uparrow}\right),\\
\dot{\mathcal{R}}_1^{\downarrow\uparrow} &= \frac{1}{m}\mathcal{P}_1^{\downarrow\uparrow},\\
\dot{\mathcal{P}}_1^{\downarrow\uparrow} &= -m\omega^2 C_1\mathcal{R}_1^{\downarrow\uparrow} - \frac{2}{3}\alpha\delta X m\tilde{\omega}^2\bar{\mathcal{R}}_1^{\downarrow\uparrow} - \frac{A}{4}\left(\chi_0\mathcal{R}_1^{\downarrow\uparrow} + \chi_1 X\bar{\mathcal{R}}_1^{\downarrow\uparrow}\right).
\end{aligned} \tag{51}$$

The energies of 2^- excitations and respective transition probabilities are listed in Table 7. The summed strength amounts to 3563.60 μ_N^2fm^2. The magnetic EWSR (40) is exhausted by 100%.

Table 7. The magnetic $K^\pi = 2^-$ excitations of ^{164}Dy.

		E_{22}, MeV	$B(M22)\uparrow$, μ_N^2fm^2
IS	SF	7.61	29.77
IV		12.02	3533.83

One can note that energies of $K^\pi = 2^-$ SF excitations (Table 7) coincide with those of $K^\pi = 0^-$ SF excitations (Table 5). It looks not surprising, because the equations describing both excitations coincide, which happens in its turn due to the neglect by the dynamics of third rank moments. As we know, taking them into account leads to the appearance of seven 1^- excitations of different nature, including the GDR (see Introduction and Figures 1 and 2). It can be expected that in this case too the above-mentioned degeneration will be removed.

4. Summary and discussion

We have found in ^{164}Dy nucleus 14 levels located in the excitation energy range of 4–17 MeV. Of these, seven are $K^\pi = 0^-$ excitations, five are $K^\pi = 1^-$, and two are $K^\pi = 2^-$.

The highest energy states are the two branches of the GDR. This is the isovector spin-scalar mode. Its isoscalar counterpart was artificially put to the zero (or very large) energy to exclude the center-of-mass motion, which represents the spurious mode. The energies of both GDR branches were described by fitting the parameters of the dipole–dipole interaction. The $K^\pi = 0^-$ and $K^\pi = 1^-$ peak positions were found at 13.01 and 16.25 MeV, respectively. The deformation-induced splitting is 3.24 MeV. These results are aligned with the established patterns observed in the physics of the GDR [10, 25]. Spin resonances induced by the spin-dipole operator (8) lie lower in energy. They are grouped in four multiplets, see Figure 5.

The excitations with $K^\pi = 2^-$ (spin index SF, energy $E_{22} = 12.02$ MeV, Table 7), $K^\pi = 1^-$ (spin index SV, energy $E_{21} = 11.97$ MeV, Table 6) and $K^\pi = 0^-$ (spin index SV, energy $E_{20} = 10.61$ MeV, Table 5) form the isovector triplet. In the spherical limit, these levels converge in one point with quantum numbers $J^\pi = 2^-$ and energy $E_2 = 10.77$ MeV (see Table 8

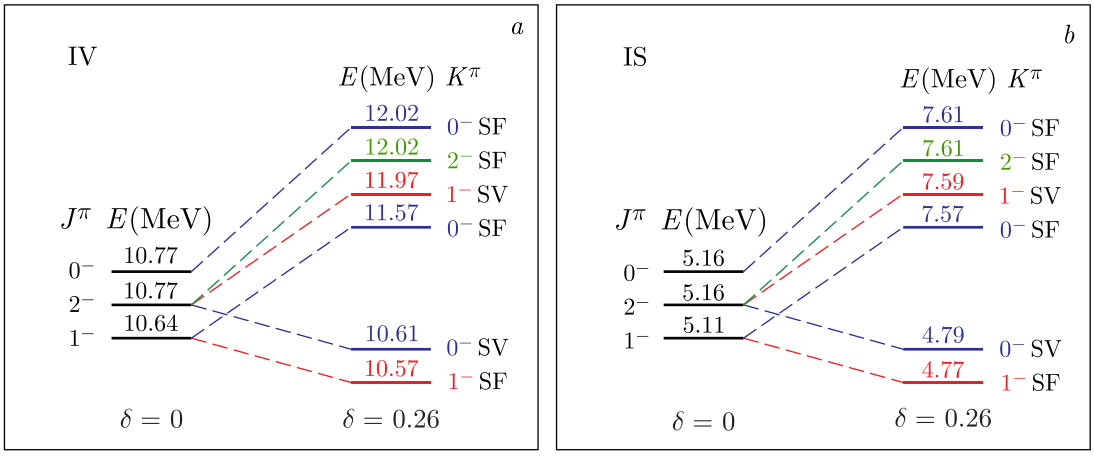

Figure 5. Energies of IV (a) and IS (b) spin-dipole excitations for $\delta = 0$ (see Table 8) and for $\delta = 0.26$ (see Tables 4–7). Calculations are performed for ^{164}Dy.

and Figure 5, *a*). The levels $K^\pi = 2^-$ and $K^\pi = 0^-$ are pure magnetic ones. Their excitation probabilities are $B(M22)\uparrow = 3533.83\ \mu_N^2\text{fm}^2$ (see Table 7) and $B(M20) = 1277.45\ \mu_N^2\text{fm}^2$ (see Table 5). The level $K^\pi = 1^-$ has the predominantly magnetic nature with the small electric admixture. The respective excitation probabilities are $B(M21)\uparrow = 1887.98\ \mu_N^2\text{fm}^2$ and $B(E11)\uparrow = 0.28\ e^2\text{fm}^2$ (see Table 6).

Table 8. The excitations of a hypothetical spherical nucleus with N and Z corresponding to ^{164}Dy.

	J^π	$E(J^\pi)$, MeV	$B(E1)\downarrow$, $e^2\text{fm}^2$	$B(M2)\downarrow$, $\mu_N^2\text{fm}^2$
IV	0^-	10.77	0	0
	1^-	10.64	0.41	0
	2^-	10.77	0	1954.06
IS	0^-	5.16	0	0
	1^-	5.11	0	0
	2^-	5.16	0	62.27

The isoscalar counterpart of this triplet is formed by the excitations with energies $E_{22} = 7.61$ MeV ($K^\pi = 2^-$, SF, Table 7), $E_{21} = 7.59$ MeV ($K^\pi = 1^-$, SV, Table 6), and $E_{20} = 4.79$ MeV ($K^\pi = 0^-$, SV, Table 5). In the spherical limit, these levels converge in one $J^\pi = 2^-$ level with the energy $E_2 = 5.16$ MeV (Table 8 and Figure 5, *b*). The levels $K^\pi = 2^-$ and $K^\pi = 0^-$ are pure magnetic ones. Their excitation probabilities $B(M22)\uparrow = 29.77\ \mu_N^2\text{fm}^2$ and $B(M20) = 141.75\ \mu_N^2\text{fm}^2$ are the order of magnitude less than in the isovector case. The level $K^\pi = 1^-$ also has the pure magnetic nature with $B(M21)\uparrow = 15.77\ \mu_N^2\text{fm}^2$. Contrary to its isovector counterpart, it has not any electric admixture. However, the last remark depends on the method of excluding the CM motion. As is seen from Table 6, in the case of zeroing CMM excitation energy this level has a little bit another energy $E_{21} = 7.65$ MeV and the nonzero (though rather small) $B(E11)$ value.

Further, the excitations with energies $E_{10} = 11.57$ MeV ($K^\pi = 0^-$, SF, Table 4) and $E_{11} = 10.57$ MeV ($K^\pi = 1^-$, SF, Table 6) form the isovector doublet. In the spherical limit these levels converge in one $J^\pi = 1^-$ level with the energy $E_1 = 10.64$ MeV, see Figure 5, *a*. The level $K^\pi = 0^-$ is pure electric one (ESDR). Its excitation probability is $B(E10) = 4.93\ e^2\text{fm}^2$ (see Table 4). The level $K^\pi = 1^-$ has the predominantly magnetic nature with the very small electric admixture. The respective excitation probabilities are $B(M21)\uparrow = 1794.12\ \mu_N^2\text{fm}^2$ and $B(E11)\uparrow = 0.17\ e^2\text{fm}^2$ (Table 6).

The isoscalar counterpart of this doublet is formed by the excitations with energies $E_{10} = 7.57$ MeV ($K^\pi = 0^-$, SF, Table 4) and $E_{11} = 4.77$ MeV ($K^\pi = 1^-$, SF, Table 6). In the spherical limit, they converge in one $J^\pi = 1^-$ level with the energy $E_1 = 5.11$ MeV (Table 8 and Figure 5, *b*). The conclusion about the electromagnetic nature of these states depends on the method of excluding the CM motion. As is seen from Table 4, the level $E_{10} = 7.57$ MeV is not excited electromagnetically in the case of the large CMM energy E_{CM}, whereas in the case of $E_{\text{CM}} = 0$ it has already a little bit another energy $E_{10} = 7.69$ MeV and the nonzero (though rather small) $B(E10)$ value. According to Table 6, the level $E_{11} = 4.77$ MeV is pure magnetic one if E_{CM} is large, whereas it acquires the electric property (though rather weak one) and the slightly another energy $E_{11} = 4.86$ MeV, if $E_{\text{CM}} = 0$.

In the case of $K^\pi = 0^-$, the electric and magnetic modes are separated. For $K^\pi = 1^-$ excitations the situation is different. In deformed nuclei, the electric and magnetic channels of

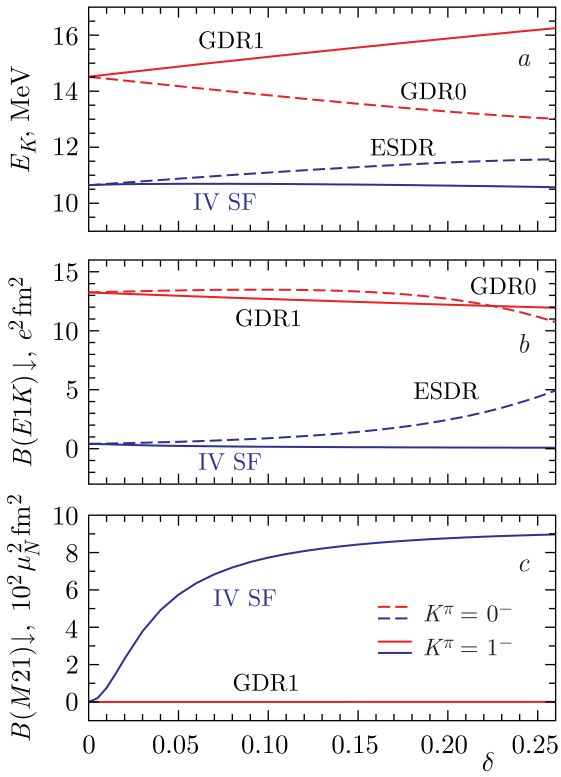

Figure 6. (a) Energies of $K^\pi = 0^-$ GDR (GDR0, red dashed line), $K^\pi = 1^-$ GDR (GDR1, red line), $K^\pi = 0^-$ ESDR (blue dashed line) and $K^\pi = 1^-$ state (IV SF, blue line) with (b) $B(E1K)$ and (c) $B(M21)$ strengths vs. deformation δ. Calculations are performed for ^{164}Dy.

1^- excitation are coupled. The result is non-zero $B(E11)$ and $B(M21)$ transition probabilities for each 1^- level, see Table 6. In the spherical limit, there is no mixing between the $J^\pi = 1^-$ and $J^\pi = 2^-$. The interplay between the GDR, ESDR (which is IV SF 0^-) and IV SF 1^- state is shown in Figure 6. It is noteworthy that the energy and $E11$ strength of the IV SF 1^- state depend weakly on the deformation, whereas the $B(M21)$, on the contrary, drops sharply, reaching zero at $\delta = 0$. It is also necessary to note the remarkable behaviour of this level with deformation: beginning at the zero deformation as the pure electric excitation with the $B(E1)\uparrow = 1.23\ e^2\text{fm}^2$, it ends at the deformation $\delta = 0.26$ as the practically pure magnetic state with the $B(E11)\uparrow = 0.17\, e^2\text{fm}^2$ and the $B(M21)\uparrow = 1794\ \mu_N^2\text{fm}^2$.

The $M2$ transition strength is dominated by the isovector response. The isoscalar one has a small contribution. It mainly makes visible the transitions in the energy range of 4–8 MeV. In the energy range above 8 MeV, the spectrum of isovector 1^- magnetic quadrupole excitations exhibits two main peaks at 10.57 MeV (SF) and 11.97 MeV (SV) with nearly equal $B(M21)$ strengths (see Table 6). Their energy centroid is at 11.29 MeV. The spectrum of isovector 0^- magnetic excitations consists of two levels at 10.61 MeV (SV) and 12.02 MeV (SF), see Table 5. Their energy centroid is at 11.06 MeV. The splitting with the 1^- bump is only 0.23 MeV. The 2^- component is represented by one strong SF state at 12.02 MeV (see Table 7).

To sum it up, the $K^\pi = 0^-$, 1^- and 2^- centroids of the isovector spin $M2$ strength are found at energies of 11.06, 11.29 and 12.02 MeV, respectively. So, the deformation-induced splitting of the $M2$ giant resonance is noticeably smaller than that of the $E1$ giant resonance. This conclusion is consistent with the results of the paper [15], where the distribution of the $M2$ strength in heavy deformed nuclei was studied within the RPA framework.

The effects of pair correlations on the $M2$ transitions in some spherical nuclei have been studied in Ref. [16]. The key observation was that the pairing interaction reduces the $M2$ strength and shifts the centroid energy to the higher region. An extension of the WFM method to include pair correlations will be done in the future.

Theoretically, the ESDR and GDR should be observed together since they have the same $J^\pi = 1^-$ value and are located in the same excitation energy region. Spherical atomic nuclei are preferred candidates for searching for the ESDR, since in this case the most pronounced gap with the GDR is expected and there is no mixing with 2^- states. It is interesting to find experimental indications to support our prediction. The collective spin-dipole excitations were the subject of interest in the paper [11], where ^{208}Pb(p, p') reaction was studied. The two states at 6.26 and 8.37 MeV were interpreted as 1^- spin-flip excitations. In a recent paper [29], photoneutron reactions on ^{208}Pb in the GDR energy region has been investigated. Several resonance structures have been detected in low-energy ^{208}Pb(γ, n) cross sections. Thus, in particular, the broad shoulder at 9.45 MeV and a prominent peak at $\sim$ 10 MeV have been observed. The ESDR position in ^{208}Pb calculated within the WFM method is 9.83 MeV [20] and can be assigned to one of the above states. The ^{208}Pb$(p, p'\gamma)$ reaction has been studied in Ref. [30]. Several discrete states of electric nature have been detected between 7 and 10 MeV. It was supposed that some of them are collective 1^- spin-flip excitations. That is certainly in line with our findings.

It is worth noting the remarkable analogy between 1^- excitations and 1^+ scissors modes, see Ref. [7]. In both cases there are four types of collective motions which are classified as isoscalar spin-scalar, isovector spin-scalar, isoscalar spin-vector and isovector spin-vector.

The rotational isoscalar spin-scalar motion is the rotation of a nucleus as a whole and represents the conservation of the nucleus angular momentum. The translational isoscalar spin-scalar motion is the linear motion of a nucleus as a whole and represents the conservation of the nucleus linear momentum.

Furthermore, the rotational isovector spin-scalar motion is the conventional scissors mode. This excitation has the appreciable admixture of the non-rotational motion (quadrupole dynamical deformations), due to which it has both magnetic and electric nonzero excitation probabilities, $B(M1)$ and $B(E2)$ respectively. The translational isovector spin-scalar motion is the GDR. This excitation has not any rotational admixture. Nevertheless, due to the spin-orbit potential it has (additionally to the electrical excitation probability $B(E1)$) the small magnetic excitation probability $B(M2)$, see Table 6.

The rotational isoscalar spin-vector motion is one of two spin scissors. It has the largest (among three scissors) magnetic dipole excitation probability $B(M1)$ and the smallest (order of magnitude) electric excitation probability $B(E2)$, see Tabe I in Ref. [7]. One can say that this scissors represents practically pure rotational motion of spin-up nucleons with respect to spin-down nucleons, the admixture of the non-rotational one being negligibly small. This means that it is practically pure magnetic mode. The translational isoscalar spin-vector motion is identified as one of 1^- excitations with the energy $E = 7.59$ MeV (see Table 6). It represents the linear oscillations of all spin-up nucleons with respect to all spin-down nucleons. It is interesting to note that, having zero $B(E11)$ and nonzero $B(M21)$, this mode also turns out pure magnetic one.

The rotational isovector spin-vector motion is the second of two spin scissors (complicated spin scissors) with a little bit smaller $B(M1)$. Its $B(E2)$ value is one order of magnitude bigger than that of the first (isoscalar spin-vector) spin scissors. This fact says that this mode has the appreciable admixture of the non-rotational motion, exactly as the conventional scissors.

The translational isovector spin-vector motion is identified as one more 1^- excitation with the energy $E = 11.97$ MeV (Table 6). It has rather big magnetic quadrupole excitation probability $B(M21) = 1887\ \mu_N^2\text{fm}^2$. Analogously to the complicated scissors, it can be described as the out-of-phase linear oscillations of spin-up protons + spin-down neutrons with respect to spin-down protons + spin-up neutrons. However, contrary to the scissors this mode has very small $B(E11)$, so one can count it as the pure magnetic one. The spin-vector motion contribution disappears in the spherical limit (like spin scissors).

Now one can say that our expectations, announced in the Introduction, concerning the possible existence of spin giant resonances of various multipolarities are justified. We have found the sought out isovector and isoscalar spin-vector giant dipole resonances.

Here is the proper place to clarify the relation between the spin-flip (SF) and spin-vector (SV) types of excitations. There exists a popular opinion that SF and SV are just the different names of the same phenomenon. See, for example, the paper [11]: "... a collective dipole spin-flip excitation ($L = 1$, $S = 1$) which in a simple collective picture can be interpreted as a collective dipole oscillation of spin-up particles against spin-down particles". However, as we have shown, SF and SV represent two different types of excitations. Moreover, the transition strengths are quite clearly separated into the spin-flip and spin-vector components.

5. Conclusions

In this work we have investigated the properties of the GDR and electric and magnetic spin-dipole resonances in heavy even-even axial deformed nuclei within the framework of the WFM method.

The energy position and splitting of the GDR caused by the deformation are calculated for ^{164}Dy. The obtained values are in good agreement with the general global trends for the GDR.

Our calculations show that spin resonance can be induced by an alternating electric field. This mode (ESDR) is low-energy satellite of the GDR and is not excited if the spin-orbit potential is neglected.

We have studied experimental 1^- spectra of spherical nuclei in search of states that could correspond to the ESDR. Several suitable candidates have been found.

Of considerable interest are spin-vector states, interpreted as collective dipole translational motion of spin "up" nucleons relative to spin "down" nucleons. These oscillations are the translational analogue of the 1^+ spin scissors mode. It was found that spin-vector displacements are generated by the spin part of the $\hat{O}(M2, 1)$ operator.

We have evaluated the energy, transition probability and deformation-induced splitting of the spin $M2$ giant resonance. The third-rank tensors are required to calculate the orbital response. However, the presented results seem vital since there are calculations indicating that the magnetic quadrupole strength is dominated by the spin response [16]. The pair correlations are another factor that influences the magnitude and distribution of $M2$ strength. The extension of the theory to include pair correlations and third-rank tensors will be considered in due course.

Acknowledgments

Valuable discussions with V. Nesterenko and R. Nazmitdinov are gratefully acknowledged.

Conflicts of interest

The authors declare no conflicts of interest.

Appendix A. Mean field

The contribution of H_{qq} (6) to the mean field potential is easily found by replacing one of the $q_{2\mu}$ operators by the average value. We have [1]

$$V_{\rm qq}^{\tau+} = \sqrt{6}\sum_{\mu}(-1)^{\mu} Z_{2-\mu}^{\tau+} q_{2\mu}, \tag{A.1}$$

where τ denotes the isospin index ($\tau = n, p$) and

$$Z_{2\mu}^{n+} = \kappa R_{2\mu}^{n+} + \bar{\kappa} R_{2\mu}^{p+}, \quad Z_{2\mu}^{p+} = \kappa R_{2\mu}^{p+} + \bar{\kappa} R_{2\mu}^{n+}. \tag{A.2}$$

The analogous expression for $H_{\rm dd}$ (5) is found in a standard way [4] with the following result for the Wigner transform of the mean field:

$$V_{\rm dd}^{n+} = \xi \mathcal{V}_{dd}^{n+} + \bar{\xi} \mathcal{V}_{\rm dd}^{p+}, \quad V_{\rm dd}^{p+} = \xi \mathcal{V}_{\rm dd}^{p+} + \bar{\xi} \mathcal{V}_{\rm dd}^{n+}, \tag{A.3}$$

with

$$\mathcal{V}_{\rm dd}^{\tau+} = \sum_{\mu=-1}^{1}(-1)^{\mu} R_{\mu}^{\tau+} r_{-\mu}, \quad \mathcal{V}_{\rm dd}^{\tau-} = \mathcal{V}_{\rm dd}^{\tau\downarrow\uparrow} = \mathcal{V}_{\rm dd}^{\tau\uparrow\downarrow} = 0. \tag{A.4}$$

For the spin-dipole mean-field potential, we derived

$$V_{\rm sd}^{\tau+} = 0, \quad V_{\rm sd}^{n\zeta} = \chi \mathcal{V}_{\rm sd}^{n\zeta} + \bar{\chi} \mathcal{V}_{\rm sd}^{p\zeta}, \quad V_{\rm sd}^{p\zeta} = \chi \mathcal{V}_{\rm sd}^{p\zeta} + \bar{\chi} \mathcal{V}_{\rm sd}^{n\zeta}, \tag{A.5}$$

where $\zeta = -, \uparrow\downarrow, \downarrow\uparrow$ and

$$\begin{aligned}
\mathcal{V}_{\rm sd}^{\tau-} &= \frac{1}{3} r_0 \left(\mathcal{M}_{2,0}^{\tau} + \frac{1}{2}\mathcal{M}_{0,0}^{\tau} \right) - \frac{1}{4}\left(r_{-1}\mathcal{M}_{2,1}^{\tau} + r_1 \mathcal{M}_{2,-1}^{\tau} \right) - \frac{1}{4}\left(r_{-1}\mathcal{E}_{1,1}^{\tau} + r_1 \mathcal{E}_{1,-1}^{\tau} \right), \\
\mathcal{V}_{\rm sd}^{\tau\downarrow\uparrow} &= -\frac{\sqrt{2}}{8} r_0 \mathcal{M}_{2,1}^{\tau} + \frac{\sqrt{2}}{12} r_1 \left(\mathcal{M}_{2,0}^{\tau} - \mathcal{M}_{0,0}^{\tau} \right) - \frac{1}{4}\left(r_1 \mathcal{E}_{1,0}^{\tau} - \frac{1}{\sqrt{2}} r_0 \mathcal{E}_{1,1}^{\tau} \right) + \frac{\sqrt{2}}{2} r_{-1} \mathcal{M}_{2,2}^{\tau}, \\
\mathcal{V}_{\rm sd}^{\tau\uparrow\downarrow} &= \frac{\sqrt{2}}{8} r_0 \mathcal{M}_{2,-1}^{\tau} - \frac{\sqrt{2}}{12} r_{-1} \left(\mathcal{M}_{2,0}^{\tau} - \mathcal{M}_{0,0}^{\tau} \right) - \frac{1}{4}\left(r_{-1}\mathcal{E}_{1,0}^{\tau} + \frac{1}{\sqrt{2}} r_0 \mathcal{E}_{1,-1}^{\tau} \right) - \frac{\sqrt{2}}{2} r_1 \mathcal{M}_{2,-2}^{\tau},
\end{aligned} \tag{A.6}$$

with denotations

$$\begin{aligned}
&\mathcal{M}_{2,1} \equiv R_1^- - \sqrt{2} R_0^{\downarrow\uparrow}, \quad \mathcal{M}_{2,-1} \equiv R_{-1}^- + \sqrt{2} R_0^{\uparrow\downarrow}, \quad \mathcal{M}_{2,0} \equiv R_0^- + \left(R_1^{\uparrow\downarrow} - R_{-1}^{\downarrow\uparrow} \right)/\sqrt{2}, \\
&\mathcal{M}_{2,2} \equiv -R_1^{\downarrow\uparrow}/\sqrt{2} \quad \mathcal{M}_{2,-2} \equiv R_{-1}^{\uparrow\downarrow}/\sqrt{2}, \quad \mathcal{M}_{0,0} \equiv R_0^- - \sqrt{2}\left(R_1^{\uparrow\downarrow} - R_{-1}^{\downarrow\uparrow} \right), \\
&\mathcal{E}_{1,1} \equiv R_1^- + \sqrt{2} R_0^{\downarrow\uparrow}, \quad \mathcal{E}_{1,-1} \equiv R_{-1}^- - \sqrt{2} R_0^{\uparrow\downarrow}, \quad \mathcal{E}_{1,0} \equiv R_1^{\uparrow\downarrow} + R_{-1}^{\downarrow\uparrow}.
\end{aligned}$$

The contribution to the mean field coming from $\sum_{\mu}(-1)^{\mu} s_{1-\mu} s_{1\mu}$ is denoted as $\mathcal{E}_{1,\mu}$, the contribution from $\sum_{\mu}(-1)^{\mu} s_{2-\mu} s_{2\mu}$ is denoted as $\mathcal{M}_{2,\mu}$, and the contribution from $s_{00} s_{00}$ is denoted as $\mathcal{M}_{0,0}$, where $s_{\lambda\mu}$ is defined by Eq. (8). Taking into account that

$$\begin{aligned}
&\mathcal{M}_{2,1} - \mathcal{E}_{1,1} = -2\sqrt{2} R_0^{\downarrow\uparrow}, \quad \mathcal{M}_{2,-1} - \mathcal{E}_{1,-1} = 2\sqrt{2} R_0^{\uparrow\downarrow}, \\
&\mathcal{M}_{2,1} + \mathcal{E}_{1,1} = 2 R_1^-, \qquad\quad \mathcal{M}_{2,-1} + \mathcal{E}_{1,-1} = 2 R_{-1}^-, \\
&\mathcal{M}_{2,0} - \mathcal{M}_{0,0} = \frac{3}{\sqrt{2}}\left(R_1^{\uparrow\downarrow} - R_{-1}^{\downarrow\uparrow} \right), \quad \mathcal{M}_{2,0} + \frac{1}{2}\mathcal{M}_{0,0} = \frac{3}{2} R_0^-,
\end{aligned}$$

we find from Eq. (A.6)

$$\mathcal{V}_{\rm sd}^{\tau\zeta} = \frac{1}{2}\left[r_0 R_0^{\tau\zeta} - r_{-1}R_1^{\tau\zeta} - r_1 R_{-1}^{\tau\zeta}\right] = \frac{1}{2}\sum_{\mu=-1}^{1}(-1)^{\mu} R_{\mu}^{\tau\zeta} r_{-\mu}. \tag{A.7}$$

Finally, we get

$$h^{\tau+} = V_{\rm qq}^{\tau+} + V_{\rm dd}^{\tau+}, \quad h^{\tau\zeta} = V_{\rm sd}^{\tau\zeta}. \tag{A.8}$$

Appendix B. Equations

Appendix B.1. $K^{\pi} = 2^{-}$ equations

$$\begin{aligned}
\dot{\bar{\mathcal{R}}}_1^{\downarrow\uparrow} &= \frac{1}{m}\bar{\mathcal{P}}_1^{\downarrow\uparrow},\\
\dot{\bar{\mathcal{P}}}_1^{\downarrow\uparrow} &= -\left(m\omega^2 - 2\kappa_0 Q_{20}\right)\bar{\mathcal{R}}_1^{\downarrow\uparrow} + 2\alpha\kappa_0\bar{Q}_{20}\mathcal{R}_1^{\downarrow\uparrow} - \frac{A}{4}\left(\chi_1\bar{\mathcal{R}}_1^{\downarrow\uparrow} + \chi_0 X\mathcal{R}_1^{\downarrow\uparrow}\right),\\
\dot{\mathcal{R}}_1^{\downarrow\uparrow} &= \frac{1}{m}\mathcal{P}_1^{\downarrow\uparrow},\\
\dot{\mathcal{P}}_1^{\downarrow\uparrow} &= -\left(m\omega^2 - 2\kappa_0 Q_{20}\right)\mathcal{R}_1^{\downarrow\uparrow} + 2\alpha\kappa_0\bar{Q}_{20}\bar{\mathcal{R}}_1^{\downarrow\uparrow} - \frac{A}{4}\left(\chi_0\mathcal{R}_1^{\downarrow\uparrow} + \chi_1 X\bar{\mathcal{R}}_1^{\downarrow\uparrow}\right),
\end{aligned} \tag{B.1}$$

where $\bar{Q}_{20} = XQ_{20}$, $X = (N-Z)/A$, $Q_{20} = Q_{00}\frac{4}{3}\delta$, $Q_{00} = A\langle r^2\rangle$, $\kappa_0 = -\dfrac{m\tilde{\omega}^2}{4Q_{00}}$ [1], $\omega^2 = \omega_0^2/[(1+\frac{4}{3}\delta)^{2/3}(1-\frac{2}{3}\delta)^{1/3}]$ with $\hbar\omega_0 = 41A^{-1/3}$. Notations $m\omega^2 C_1 = m\omega^2 - 2\kappa_0 Q_{20}$ and $m\omega^2 C_0 = m\omega^2 + 4\kappa_0 Q_{20}$ are used in the main text of the paper, see Subsection 3.1.

Appendix B.2. $K^{\pi} = 1^{-}$ equations

$$\begin{aligned}
\dot{\bar{\mathcal{R}}}_1^{+} &= \frac{1}{m}\bar{\mathcal{P}}_1^{+} - i\hbar\frac{\eta}{2}\left(\bar{\mathcal{R}}_1^{-} + \sqrt{2}\bar{\mathcal{R}}_0^{\downarrow\uparrow}\right),\\
\dot{\bar{\mathcal{R}}}_1^{-} &= \frac{1}{m}\bar{\mathcal{P}}_1^{-} - i\hbar\frac{\eta}{2}\bar{\mathcal{R}}_1^{+},\\
\dot{\bar{\mathcal{R}}}_0^{\downarrow\uparrow} &= \frac{1}{m}\bar{\mathcal{P}}_0^{\downarrow\uparrow} - i\hbar\frac{\eta}{2\sqrt{2}}\bar{\mathcal{R}}_1^{+},\\
\dot{\bar{\mathcal{P}}}_1^{+} &= -\left(m\omega^2 - 2\kappa_0 Q_{20}\right)\bar{\mathcal{R}}_1^{+} - i\hbar\frac{\eta}{2}\left(\bar{\mathcal{P}}_1^{-} + \sqrt{2}\bar{\mathcal{P}}_0^{\downarrow\uparrow}\right) + 2\alpha\kappa_0\bar{Q}_{20}\mathcal{R}_1^{+} - A\left(\xi_1^{K=1}\bar{\mathcal{R}}_1^{+} + \xi_0^{K=1}X\mathcal{R}_1^{+}\right),\\
\dot{\bar{\mathcal{P}}}_1^{-} &= -\left(m\omega^2 - 2\kappa_0 Q_{20}\right)\bar{\mathcal{R}}_1^{-} - i\hbar\frac{\eta}{2}\bar{\mathcal{P}}_1^{+} + 2\alpha\kappa_0\bar{Q}_{20}\mathcal{R}_1^{-} - \frac{A}{4}\left(\chi_1\bar{\mathcal{R}}_1^{-} + \chi_0 X\mathcal{R}_1^{-}\right),\\
\dot{\bar{\mathcal{P}}}_0^{\downarrow\uparrow} &= -\left(m\omega^2 + 4\kappa_0 Q_{20}\right)\bar{\mathcal{R}}_0^{\downarrow\uparrow} - i\hbar\frac{\eta}{2\sqrt{2}}\bar{\mathcal{P}}_1^{+} - 4\alpha\kappa_0\bar{Q}_{20}\mathcal{R}_0^{\downarrow\uparrow} - \frac{A}{4}\left(\chi_1\bar{\mathcal{R}}_0^{\downarrow\uparrow} + \chi_0 X\mathcal{R}_0^{\downarrow\uparrow}\right),\\
\dot{\mathcal{R}}_1^{+} &= \frac{1}{m}\mathcal{P}_1^{+} - i\hbar\frac{\eta}{2}\left(\mathcal{R}_1^{-} + \sqrt{2}\mathcal{R}_0^{\downarrow\uparrow}\right),\\
\dot{\mathcal{R}}_1^{-} &= \frac{1}{m}\mathcal{P}_1^{-} - i\hbar\frac{\eta}{2}\mathcal{R}_1^{+},\\
\dot{\mathcal{R}}_0^{\downarrow\uparrow} &= \frac{1}{m}\mathcal{P}_0^{\downarrow\uparrow} - i\hbar\frac{\eta}{2\sqrt{2}}\mathcal{R}_1^{+},
\end{aligned}$$

$$\dot{\mathcal{P}}_1^+ = -\left(m\omega^2 - 2\kappa_0 Q_{20}\right)\mathcal{R}_1^+ - i\hbar\frac{\eta}{2}\left(\mathcal{P}_1^- + \sqrt{2}\mathcal{P}_0^{\downarrow\uparrow}\right) + 2\alpha\kappa_0\bar{Q}_{20}\bar{\mathcal{R}}_1^+ - A\left(\xi_0^{K=1}\mathcal{R}_1^+ + \xi_1^{K=1}X\bar{\mathcal{R}}_1^+\right),$$

$$\dot{\mathcal{P}}_1^- = -\left(m\omega^2 - 2\kappa_0 Q_{20}\right)\mathcal{R}_1^- - i\hbar\frac{\eta}{2}\mathcal{P}_1^+ + 2\alpha\kappa_0\bar{Q}_{20}\bar{\mathcal{R}}_1^- - \frac{A}{4}\left(\chi_0\mathcal{R}_1^- + \chi_1 X\bar{\mathcal{R}}_1^-\right),$$

$$\dot{\mathcal{P}}_0^{\downarrow\uparrow} = -\left(m\omega^2 + 4\kappa_0 Q_{20}\right)\mathcal{R}_0^{\downarrow\uparrow} - i\hbar\frac{\eta}{2\sqrt{2}}\mathcal{P}_1^+ - 4\alpha\kappa_0\bar{Q}_{20}\bar{\mathcal{R}}_0^{\downarrow\uparrow} - \frac{A}{4}\left(\chi_0\mathcal{R}_0^{\downarrow\uparrow} + \chi_1 X\bar{\mathcal{R}}_0^{\downarrow\uparrow}\right), \qquad \text{(B.2)}$$

where $\hbar^2\eta = 2\hbar\omega_0\kappa_{\rm N}$ [21, 22] and $\kappa_{\rm N}$ is Nilsson spin-orbit strength constant.

Appendix B.3. $K^\pi = 0^-$ equations

$$\dot{\bar{\mathcal{R}}}_0^+ = \frac{1}{m}\bar{\mathcal{P}}_0^+ - i\hbar\frac{\eta}{2}\sqrt{2}\left(\bar{\mathcal{R}}_1^{\uparrow\downarrow} + \bar{\mathcal{R}}_{-1}^{\downarrow\uparrow}\right),$$

$$\dot{\bar{\mathcal{R}}}_0^- = \frac{1}{m}\bar{\mathcal{P}}_0^-,$$

$$\dot{\bar{\mathcal{R}}}_1^{\uparrow\downarrow} = \frac{1}{m}\bar{\mathcal{P}}_1^{\uparrow\downarrow} - i\hbar\frac{\eta}{2\sqrt{2}}\bar{\mathcal{R}}_0^+,$$

$$\dot{\bar{\mathcal{R}}}_{-1}^{\downarrow\uparrow} = \frac{1}{m}\bar{\mathcal{P}}_{-1}^{\downarrow\uparrow} - i\hbar\frac{\eta}{2\sqrt{2}}\bar{\mathcal{R}}_0^+,$$

$$\dot{\bar{\mathcal{P}}}_0^+ = -\left(m\omega^2 + 4\kappa_0 Q_{20}\right)\bar{\mathcal{R}}_0^+ - i\hbar\frac{\eta}{2}\sqrt{2}\left(\bar{\mathcal{P}}_1^{\uparrow\downarrow} + \bar{\mathcal{P}}_{-1}^{\downarrow\uparrow}\right) - 4\alpha\kappa_0\bar{Q}_{20}\mathcal{R}_0^+ - A\left(\xi_1^{K=0}\bar{\mathcal{R}}_0^+ + \xi_0^{K=0}X\mathcal{R}_0^+\right),$$

$$\dot{\bar{\mathcal{P}}}_0^- = -\left(m\omega^2 + 4\kappa_0 Q_{20}\right)\bar{\mathcal{R}}_0^- - 4\alpha\kappa_0\bar{Q}_{20}\mathcal{R}_0^- - \frac{A}{4}\left(\chi_1\bar{\mathcal{R}}_0^- + \chi_0 X\mathcal{R}_0^-\right),$$

$$\dot{\bar{\mathcal{P}}}_1^{\uparrow\downarrow} = -\left(m\omega^2 - 2\kappa_0 Q_{20}\right)\bar{\mathcal{R}}_1^{\uparrow\downarrow} - i\hbar\frac{\eta}{2\sqrt{2}}\bar{\mathcal{P}}_0^+ + 2\alpha\kappa_0\bar{Q}_{20}\mathcal{R}_1^{\uparrow\downarrow} - \frac{A}{4}\left(\chi_1\bar{\mathcal{R}}_1^{\uparrow\downarrow} + \chi_0 X\mathcal{R}_1^{\uparrow\downarrow}\right),$$

$$\dot{\bar{\mathcal{P}}}_{-1}^{\downarrow\uparrow} = -\left(m\omega^2 - 2\kappa_0 Q_{20}\right)\bar{\mathcal{R}}_{-1}^{\downarrow\uparrow} - i\hbar\frac{\eta}{2\sqrt{2}}\bar{\mathcal{P}}_0^+ + 2\alpha\kappa_0\bar{Q}_{20}\mathcal{R}_{-1}^{\downarrow\uparrow} - \frac{A}{4}\left(\chi_1\bar{\mathcal{R}}_{-1}^{\downarrow\uparrow} + \chi_0 X\mathcal{R}_{-1}^{\uparrow\downarrow}\right),$$

$$\dot{\mathcal{R}}_0^+ = \frac{1}{m}\mathcal{P}_0^+ - i\hbar\frac{\eta}{2}\sqrt{2}\left(\mathcal{R}_1^{\uparrow\downarrow} + \mathcal{R}_{-1}^{\downarrow\uparrow}\right),$$

$$\dot{\mathcal{R}}_0^- = \frac{1}{m}\mathcal{P}_0^-,$$

$$\dot{\mathcal{R}}_1^{\uparrow\downarrow} = \frac{1}{m}\mathcal{P}_1^{\uparrow\downarrow} - i\hbar\frac{\eta}{2\sqrt{2}}\mathcal{R}_0^+,$$

$$\dot{\mathcal{R}}_{-1}^{\downarrow\uparrow} = \frac{1}{m}\mathcal{P}_{-1}^{\downarrow\uparrow} - i\hbar\frac{\eta}{2\sqrt{2}}\mathcal{R}_0^+,$$

$$\dot{\mathcal{P}}_0^+ = -\left(m\omega^2 + 4\kappa_0 Q_{20}\right)\mathcal{R}_0^+ - i\hbar\frac{\eta}{2}\sqrt{2}\left(\mathcal{P}_1^{\uparrow\downarrow} + \mathcal{P}_{-1}^{\downarrow\uparrow}\right) - 4\alpha\kappa_0\bar{Q}_{20}\bar{\mathcal{R}}_0^+ - A\left(\xi_0^{K=0}\mathcal{R}_0^+ + \xi_1^{K=0}X\bar{\mathcal{R}}_0^+\right),$$

$$\dot{\mathcal{P}}_0^- = -\left(m\omega^2 + 4\kappa_0 Q_{20}\right)\mathcal{R}_0^- - 4\alpha\kappa_0\bar{Q}_{20}\bar{\mathcal{R}}_0^- - \frac{A}{4}\left(\chi_0\mathcal{R}_0^- + \chi_1 X\bar{\mathcal{R}}_0^-\right),$$

$$\dot{\mathcal{P}}_1^{\uparrow\downarrow} = -\left(m\omega^2 - 2\kappa_0 Q_{20}\right)\mathcal{R}_1^{\uparrow\downarrow} - i\hbar\frac{\eta}{2\sqrt{2}}\mathcal{P}_0^+ + 2\alpha\kappa_0\bar{Q}_{20}\bar{\mathcal{R}}_1^{\uparrow\downarrow} - \frac{A}{4}\left(\chi_0\mathcal{R}_1^{\uparrow\downarrow} + \chi_1 X\bar{\mathcal{R}}_1^{\uparrow\downarrow}\right),$$

$$\dot{\mathcal{P}}_{-1}^{\downarrow\uparrow} = -\left(m\omega^2 - 2\kappa_0 Q_{20}\right)\mathcal{R}_{-1}^{\downarrow\uparrow} - i\hbar\frac{\eta}{2\sqrt{2}}\mathcal{P}_0^+ + 2\alpha\kappa_0\bar{Q}_{20}\bar{\mathcal{R}}_{-1}^{\downarrow\uparrow} - \frac{A}{4}\left(\chi_0\mathcal{R}_{-1}^{\downarrow\uparrow} + \chi_1 X\bar{\mathcal{R}}_{-1}^{\uparrow\downarrow}\right). \qquad \text{(B.3)}$$

Appendix B.3.1. Electric $K^\pi = 0^-$

$$
\begin{aligned}
\dot{\bar{\mathcal{R}}}_0^+ &= \frac{1}{m}\bar{\mathcal{P}}_0^+ - i\hbar\frac{\eta}{\sqrt{2}}\bar{\mathcal{R}}_0^E,\\
\dot{\bar{\mathcal{R}}}_0^E &= \frac{1}{m}\bar{\mathcal{P}}_0^E - i\hbar\frac{\eta}{\sqrt{2}}\bar{\mathcal{R}}_0^+,\\
\dot{\bar{\mathcal{P}}}_0^+ &= -m\omega^2 C_0\bar{\mathcal{R}}_0^+ - i\hbar\frac{\eta}{\sqrt{2}}\bar{P}_0^E + \frac{4}{3}\alpha\delta X m\tilde{\omega}^2\mathcal{R}_0^+ - A\left(\xi_1^{K=0}\bar{\mathcal{R}}_0^+ + \xi_0^{K=0}X\mathcal{R}_0^+\right),\\
\dot{\bar{\mathcal{P}}}_0^E &= -m\omega^2 C_1\bar{\mathcal{R}}_0^E - i\hbar\frac{\eta}{\sqrt{2}}\bar{\mathcal{P}}_0^+ - \frac{2}{3}\alpha\delta X m\tilde{\omega}^2\mathcal{R}_0^E - \frac{A}{4}\left(\chi_1\bar{\mathcal{R}}_0^E + \chi_0 X\mathcal{R}_0^E\right),\\
\dot{\mathcal{R}}_0^+ &= \frac{1}{m}\mathcal{P}_0^+ - i\hbar\frac{\eta}{\sqrt{2}}\mathcal{R}_0^E,\\
\dot{\mathcal{R}}_0^E &= \frac{1}{m}\mathcal{P}_0^E - i\hbar\frac{\eta}{\sqrt{2}}\mathcal{R}_0^+,\\
\dot{\mathcal{P}}_0^+ &= -m\omega^2 C_0\mathcal{R}_0^+ - i\hbar\frac{\eta}{\sqrt{2}}\mathcal{P}_0^E + \frac{4}{3}\alpha\delta X m\tilde{\omega}^2\bar{\mathcal{R}}_0^+ - A\left(\xi_0^{K=0}\mathcal{R}_0^+ + \xi_1^{K=0}X\bar{\mathcal{R}}_0^+\right),\\
\dot{\mathcal{P}}_0^E &= -m\omega^2 C_1\mathcal{R}_0^E - i\hbar\frac{\eta}{\sqrt{2}}\mathcal{P}_0^+ - \frac{2}{3}\alpha\delta X m\tilde{\omega}^2\bar{\mathcal{R}}_0^E - \frac{A}{4}\left(\chi_0\mathcal{R}_0^E + \chi_1 X\bar{R}_0^E\right),
\end{aligned}
\tag{B.4}
$$

where $\mathcal{R}_0^E = \mathcal{R}_1^{\uparrow\downarrow} + \mathcal{R}_{-1}^{\downarrow\uparrow}$, $\mathcal{P}_0^E = \mathcal{P}_1^{\uparrow\downarrow} + \mathcal{P}_{-1}^{\downarrow\uparrow}$.

Appendix B.3.2. Magnetic $K^\pi = 0^-$

$$
\begin{aligned}
\dot{\bar{\mathcal{R}}}_0^- &= \frac{1}{m}\bar{\mathcal{P}}_0^-,\\
\dot{\bar{\mathcal{P}}}_0^- &= -m\omega^2 C_0\bar{\mathcal{R}}_0^- + \frac{4}{3}\alpha\delta X m\tilde{\omega}^2\mathcal{R}_0^- - \frac{A}{4}\left(\chi_1\bar{\mathcal{R}}_0^- + \chi_0 X\mathcal{R}_0^-\right),\\
\dot{\mathcal{R}}_0^- &= \frac{1}{m}\mathcal{P}_0^-,\\
\dot{\mathcal{P}}_0^- &= -m\omega^2 C_0\mathcal{R}_0^- + \frac{4}{3}\alpha\delta X m\tilde{\omega}^2\bar{\mathcal{R}}_0^- - \frac{A}{4}\left(\chi_0\mathcal{R}_0^- + \chi_1 X\bar{\mathcal{R}}_0^-\right),
\end{aligned}
\tag{B.5}
$$

$$
\begin{aligned}
\dot{\bar{\mathcal{R}}}_0^M &= \frac{1}{m}\bar{\mathcal{P}}_0^M,\\
\dot{\bar{\mathcal{P}}}_0^M &= -m\omega^2 C_1\bar{\mathcal{R}}_0^M - \frac{2}{3}\alpha\delta X m\tilde{\omega}^2\mathcal{R}_0^M - \frac{A}{4}\left(\chi_1\bar{\mathcal{R}}_0^M + \chi_0 X\mathcal{R}_0^M\right),\\
\dot{\mathcal{R}}_0^M &= \frac{1}{m}\mathcal{P}_0^M,\\
\dot{\mathcal{P}}_0^M &= -m\omega^2 C_1\mathcal{R}_0^M - \frac{2}{3}\alpha\delta X m\tilde{\omega}^2\bar{\mathcal{R}}_0^M - \frac{A}{4}\left(\chi_0\mathcal{R}_0^M + \chi_1 X\bar{\mathcal{R}}_0^M\right),
\end{aligned}
\tag{B.6}
$$

where $\mathcal{R}_0^M = \mathcal{R}_1^{\uparrow\downarrow} - \mathcal{R}_{-1}^{\downarrow\uparrow}$, $\mathcal{P}_0^M = \mathcal{P}_1^{\uparrow\downarrow} - \mathcal{P}_{-1}^{\downarrow\uparrow}$.

Appendix C. Electromagnetic transition probabilities

Excitation probabilities are calculated with the help of the theory of linear response of the system to a weak external field

$$\hat{O}(t) = \hat{O}\,\mathrm{e}^{-i\Omega t} + \hat{O}^{\dagger}\,\mathrm{e}^{i\Omega t}. \tag{C.1}$$

A detailed explanation can be found in [1, 7]. We recall only the main points. The matrix elements of the operator $\hat{O}$ obey the relationship [31]

$$|\langle\psi_a|\hat{O}|\psi_0\rangle|^2 = \hbar \lim_{\Omega\to\Omega_a}(\Omega-\Omega_a)\overline{\langle\psi'|\hat{O}|\psi'\rangle \mathrm{e}^{-i\Omega t}}, \tag{C.2}$$

where ψ_0 and ψ_a are the stationary wave functions of the unperturbed ground and excited states; ψ' is the wave function of the perturbed ground state; $\Omega_a = (E_a - E_0)/\hbar$ are the normal frequencies; the bar means averaging over a time interval much larger than $1/\Omega$.

Appendix C.1. Electric dipole transitions

To calculate the electric dipole transition probability, it is necessary to excite the system by the following external field:

$$\hat{O}(E1,\mu) = e\sum_{\tau}\left(\frac{Z}{A}\delta_{\tau n} - \frac{N}{A}\delta_{\tau p}\right) r_{\tau} Y_{1\mu}(\hat{\mathbf{r}}_{\tau}). \tag{C.3}$$

The electric dipole operator (C.3) in cyclic coordinates r_μ reads

$$\hat{O}(E1,\mu) = e\sqrt{\frac{3}{4\pi}}\sum_{\tau}\left(\frac{Z}{A}\delta_{\tau n} - \frac{N}{A}\delta_{\tau p}\right) [r_{\mu}]_{\tau}. \tag{C.4}$$

The reduced probability for electric dipole transition reads

$$B(E1\mu)_a = |\langle\psi_a|\hat{O}(E1,\mu)|\psi_0\rangle|^2 = \hbar \lim_{\Omega\to\Omega_a}(\Omega-\Omega_a)\overline{\langle\psi'|\hat{O}(E1,\mu)|\psi'\rangle \mathrm{e}^{-i\Omega t}}. \tag{C.5}$$

For the matrix element, we have

$$\langle\psi'|\hat{O}(E1,\mu)|\psi'\rangle = e\sqrt{\frac{3}{4\pi}}\left[\frac{Z}{A}\mathcal{R}^{\mathrm{n}}_{\mu} - \frac{N}{A}\mathcal{R}^{\mathrm{p}}_{\mu}\right] = \frac{e}{2}\sqrt{\frac{3}{4\pi}}\left[\bar{\mathcal{R}}^{+}_{\mu} - X\mathcal{R}^{+}_{\mu}\right]. \tag{C.6}$$

Due to the external field (C.4), dynamical equations for collective variables $\mathcal{P}^{n+}_{\mu}$ and $\mathcal{P}^{p+}_{\mu}$ become inhomogeneous:

$$\begin{aligned}
\dot{\mathcal{P}}^{n+}_{\mu} &= \ldots + e\sqrt{\frac{3}{4\pi}}\frac{NZ}{A}\,\mathrm{e}^{i\Omega t},\\
\dot{\mathcal{P}}^{p+}_{\mu} &= \ldots - e\sqrt{\frac{3}{4\pi}}\frac{NZ}{A}\,\mathrm{e}^{i\Omega t}.
\end{aligned} \tag{C.7}$$

As a result, for $\bar{\mathcal{P}}^{+}_{\mu} = \mathcal{P}^{n+}_{\mu} - \mathcal{P}^{p+}_{\mu}$ we obtain

$$\dot{\bar{\mathcal{P}}}^{+}_{\mu} = \ldots + 2e\sqrt{\frac{3}{4\pi}}\frac{NZ}{A}\,\mathrm{e}^{i\Omega t}. \tag{C.8}$$

Solving the inhomogeneous set of equations, one can find the values of $\bar{\mathcal{R}}^{+}_{\mu}$ and $\mathcal{R}^{+}_{\mu}$ required in (C.5), (C.6) and calculate $B(E1\mu)$ factors for all excitations as explained in [1, 7].

Appendix C.2. Magnetic transitions

To calculate the magnetic transition probability, it is necessary to excite the system by the following external field:

$$\hat{O}(M\lambda,\mu)=\mu_N\sum_k^A\left(g_s(k)\hat{\mathbf{S}}_k+\frac{2}{\lambda+1}g_l(k)\hat{\mathbf{l}}_k\right)\cdot\nabla_k\left(r_k^\lambda Y_{\lambda\mu}(\hat{\mathbf{r}}_k)\right). \tag{C.9}$$

The free particle g-factors are given by $g_l^p=1$, $g_s^p=5.5856$ for protons and $g_l^n=0$, $g_s^n=-3.8263$ for neutrons, $g_s^{\rm IV}=g_s^n-g_s^p$, $g_s^{\rm IS}=g_s^n+g_s^p$. The spin quenching factor q can be applied in the calculations: $g_s^\tau=qg_s^{\tau\rm free}$. The reduced probability for $M\lambda$ magnetic transition reads

$$B(M\lambda\mu)_a=|\langle\psi_a|\hat{O}(M\lambda,\mu)|\psi_0\rangle|^2=\hbar\lim_{\Omega\to\Omega_a}(\Omega-\Omega_a)\overline{\langle\psi'|\hat{O}(M\lambda,\mu)|\psi'\rangle e^{-i\Omega t}}. \tag{C.10}$$

The $\hat{O}(M2,\mu)$ operator in cyclic coordinates reads

$$\hat{O}(M2,\mu)=\mu_N\sqrt{\frac{15}{2\pi}}\sum_k^A\sum_{\nu=-1}^1 C^{2\mu}_{1(\mu-\nu),1\nu}\left[g_s\hat{S}_\nu r_{\mu-\nu}+\frac{2}{3}g_l\hat{l}_\nu r_{\mu-\nu}\right]_k. \tag{C.11}$$

For the matrix element, we have

$$\langle\psi'|\hat{O}(M2,\mu)|\psi'\rangle=\mu_N\sqrt{\frac{15}{2\pi}}\sum_k^A\sum_{\nu=-1}^1 C^{2\mu}_{1(\mu-\nu),1\nu}\left[g_s\sum_{\sigma,\sigma'}\langle\sigma|\hat{S}_\nu|\sigma'\rangle\mathcal{R}^{\sigma'\sigma}_{\mu-\nu}-i\frac{2\sqrt{2}}{3}g_l\mathcal{T}^+_{1\nu,\mu-\nu}\right]_k, \tag{C.12}$$

where

$$\mathcal{T}^+_{\lambda\mu,\nu}(t)=(2\pi\hbar)^{-3}\int d\mathbf{r}\int d\mathbf{p}\,\{r\otimes p\}_{\lambda\mu}r_\nu\,\delta f^+(\mathbf{r},\mathbf{p},t). \tag{C.13}$$

Only the dynamics of tensors of the first rank in the coordinate and momentum are taken into account in this work. In this formulation of the problem, only the spin contribution of the operator $\hat{O}(M2,\mu)$ can be estimated:

$$\langle\psi'|\hat{O}_S(M2,\mu)|\psi'\rangle=\mu_N\sqrt{\frac{15}{2\pi}}\sum_{\tau=n,p}g_s^\tau\sum_{\nu=-1}^1 C^{2\mu}_{1(\mu-\nu),1\nu}\left[\sum_{\sigma,\sigma'}\langle\sigma|\hat{S}_\nu|\sigma'\rangle\mathcal{R}^{\sigma'\sigma}_{\mu-\nu}\right]_\tau. \tag{C.14}$$

From Eq. (C.14), for the $\mu=0,1,2$ components we obtain

$$\langle\psi'|\hat{O}_S(M2,0)|\psi'\rangle=\mu_N\sqrt{\frac{5}{4\pi}}\hbar\sum_{\tau=n,p}g_s^\tau\left[\mathcal{R}_0^{\tau-}+\frac{1}{\sqrt{2}}\left(\mathcal{R}_1^{\tau\uparrow\downarrow}-\mathcal{R}_{-1}^{\tau\downarrow\uparrow}\right)\right], \tag{C.15}$$

$$\langle\psi'|\hat{O}_S(M2,1)|\psi'\rangle=\mu_N\sqrt{\frac{15}{16\pi}}\hbar\sum_{\tau=n,p}g_s^\tau\left[\mathcal{R}_1^{\tau-}-\sqrt{2}\,\mathcal{R}_0^{\tau\downarrow\uparrow}\right], \tag{C.16}$$

$$\langle\psi'|\hat{O}_S(M2,2)|\psi'\rangle=-\mu_N\sqrt{\frac{15}{4\pi}}\hbar\sum_{\tau=n,p}g_s^\tau\mathcal{R}_1^{\tau\downarrow\uparrow}. \tag{C.17}$$

The matrix elements $\langle\psi'|\hat{O}_S(M2,\mu)|\psi'\rangle$ in terms of isoscalar and isovector variables have the following form:

$$\langle\psi'|\hat{O}_S(M2,0)|\psi'\rangle = \mu_N\frac{\hbar}{2}\sqrt{\frac{5}{4\pi}}\left[g_s^{\rm IS}\left(\mathcal{R}_0^- + \frac{\mathcal{R}_1^{\uparrow\downarrow} - \mathcal{R}_{-1}^{\downarrow\uparrow}}{\sqrt{2}}\right) + g_s^{\rm IV}\left(\bar{\mathcal{R}}_0^- + \frac{\bar{\mathcal{R}}_1^{\uparrow\downarrow} - \bar{\mathcal{R}}_{-1}^{\downarrow\uparrow}}{\sqrt{2}}\right)\right], \quad \text{(C.18)}$$

$$\langle\psi'|\hat{O}_S(M2,1)|\psi'\rangle = \mu_N\frac{\hbar}{2}\sqrt{\frac{15}{16\pi}}\left[g_s^{\rm IS}\left(\mathcal{R}_1^- - \sqrt{2}\,\mathcal{R}_0^{\downarrow\uparrow}\right) + g_s^{\rm IV}\left(\bar{\mathcal{R}}_1^- - \sqrt{2}\,\bar{\mathcal{R}}_0^{\downarrow\uparrow}\right)\right], \quad \text{(C.19)}$$

$$\langle\psi'|\hat{O}_S(M2,2)|\psi'\rangle = -\mu_N\frac{\hbar}{2}\sqrt{\frac{15}{4\pi}}\left[g_s^{\rm IS}\mathcal{R}_1^{\downarrow\uparrow} + g_s^{\rm IV}\bar{\mathcal{R}}_1^{\downarrow\uparrow}\right]. \quad \text{(C.20)}$$

Since $g_s^{\rm IV} = 9.4119$ is much larger than $g_s^{\rm IS} = 1.7593$, the magnetic multipole operator is dominantly isovector in nature.

Due to the external field (C.11), some dynamical equations become inhomogeneous:

$$\begin{aligned}
\dot{\mathcal{P}}_1^{\tau-} &= \ldots + \mu_N\hbar\sqrt{\frac{15}{4\pi}}\frac{g_s^\tau}{2}N^\tau\,{\rm e}^{i\Omega t},\\
\dot{\mathcal{P}}_0^{\tau\downarrow\uparrow} &= \ldots - \mu_N\hbar\sqrt{\frac{15}{8\pi}}\frac{g_s^\tau}{2}N^\tau\,{\rm e}^{i\Omega t},\\
\dot{\mathcal{P}}_1^{\tau\downarrow\uparrow} &= \ldots + \mu_N\hbar\sqrt{\frac{15}{4\pi}}\frac{g_s^\tau}{2}N^\tau\,{\rm e}^{i\Omega t},\\
\dot{\mathcal{P}}_0^{\tau-} &= \ldots - \mu_N\hbar\sqrt{\frac{5}{4\pi}}g_s^\tau N^\tau\,{\rm e}^{i\Omega t},\\
\dot{\mathcal{P}}_1^{\tau\uparrow\downarrow} &= \ldots - \mu_N\hbar\sqrt{\frac{5}{8\pi}}\frac{g_s^\tau}{2}N^\tau\,{\rm e}^{i\Omega t},\\
\dot{\mathcal{P}}_{-1}^{\tau\downarrow\uparrow} &= \ldots + \mu_N\hbar\sqrt{\frac{5}{8\pi}}\frac{g_s^\tau}{2}N^\tau\,{\rm e}^{i\Omega t},
\end{aligned} \quad \text{(C.21)}$$

where $N^\tau = N$ for $\tau = n$ and $N^\tau = Z$ for $\tau = p$. As a result, for isovector and isoscalar equations from (B.1), (B.2) and (B.3) we obtain

$$\begin{aligned}
\dot{\bar{\mathcal{P}}}_1^- &= \ldots + \mu_N\hbar\sqrt{\frac{15}{4\pi}}\frac{A}{4}\left(g_s^{\rm IV} + Xg_s^{\rm IS}\right){\rm e}^{i\Omega t},\\
\dot{\mathcal{P}}_1^- &= \ldots + \mu_N\hbar\sqrt{\frac{15}{4\pi}}\frac{A}{4}\left(g_s^{\rm IS} + Xg_s^{\rm IV}\right){\rm e}^{i\Omega t},\\
\dot{\bar{\mathcal{P}}}_0^{\downarrow\uparrow} &= \ldots - \mu_N\hbar\sqrt{\frac{15}{8\pi}}\frac{A}{4}\left(g_s^{\rm IV} + Xg_s^{\rm IS}\right){\rm e}^{i\Omega t},\\
\dot{\mathcal{P}}_0^{\downarrow\uparrow} &= \ldots - \mu_N\hbar\sqrt{\frac{15}{8\pi}}\frac{A}{4}\left(g_s^{\rm IS} + Xg_s^{\rm IV}\right){\rm e}^{i\Omega t},\\
\dot{\bar{\mathcal{P}}}_1^{\downarrow\uparrow} &= \ldots + \mu_N\hbar\sqrt{\frac{15}{4\pi}}\frac{A}{4}\left(g_s^{\rm IV} + Xg_s^{\rm IS}\right){\rm e}^{i\Omega t},\\
\dot{\mathcal{P}}_1^{\downarrow\uparrow} &= \ldots + \mu_N\hbar\sqrt{\frac{15}{4\pi}}\frac{A}{4}\left(g_s^{\rm IS} + Xg_s^{\rm IV}\right){\rm e}^{i\Omega t},
\end{aligned}$$

$$\dot{\mathcal{P}}_0^- = \ldots - \mu_N\hbar\sqrt{\frac{5}{4\pi}}\frac{A}{2}\left(g_s^{\rm IV} + Xg_s^{\rm IS}\right)\ {\rm e}^{i\Omega t},$$

$$\dot{\mathcal{P}}_0^- = \ldots - \mu_N\hbar\sqrt{\frac{5}{4\pi}}\frac{A}{2}\left(g_s^{\rm IS} + Xg_s^{\rm IV}\right)\ {\rm e}^{i\Omega t},$$

$$\dot{\bar{\mathcal{P}}}_0^M = \ldots - \mu_N\hbar\sqrt{\frac{5}{8\pi}}\frac{A}{2}\left(g_s^{\rm IV} + Xg_s^{\rm IS}\right)\ {\rm e}^{i\Omega t},$$

$$\dot{\mathcal{P}}_0^M = \ldots - \mu_N\hbar\sqrt{\frac{5}{8\pi}}\frac{A}{2}\left(g_s^{\rm IS} + Xg_s^{\rm IV}\right)\ {\rm e}^{i\Omega t}. \qquad \text{(C.22)}$$

Solving the inhomogeneous sets of equations (C.22), one can find the values of $\bar{\mathcal{R}}_\mu^\zeta$ and $\mathcal{R}_\mu^\zeta$ ($\zeta = -, \uparrow\downarrow, \downarrow\uparrow$) required in (C.18), (C.19), (C.20) and calculate $B(M2\mu)$ factors.

References

[1] E. B. Balbutsev and P. Schuck, The nuclear scissors mode in a solvable model, Nucl. Phys. A 720 (2003) 293–336 [Erratum *ibid.* 728 (2003) 471–479]. https://doi.org/10.1016/S0375-9474(03)01078-9.

[2] E. B. Balbutsev and P. Schuck, The nuclear scissors mode from various aspects, Ann. Phys. 322 (2007) 489–529. https://doi.org/10.1134/1.2053333.

[3] E. B. Balbutsev, I. V. Molodtsova, and P. Schuck, Spin scissors mode and the fine structure of $M1$ states in nuclei, Nucl. Phys. A 872 (2011) 42–68. https://doi.org/10.1016/j.nuclphysa.2011.09.013.

[4] E. B. Balbutsev, I. V. Molodtsova, and P. Schuck, New type of nuclear collective motion: The spin scissors mode, Phys. Rev. C 88 (2013) 014306-(1–18), https://doi.org/10.1103/PhysRevC.88.014306.

[5] E. B. Balbutsev, I. V. Molodtsova, and P. Schuck, Orbital and spin scissors modes in superfluid nuclei, Phys. Rev. C 91 (2015) 064312-(1–20). https://doi.org/10.1103/PhysRevC.91.064312.

[6] E. B. Balbutsev, I. V. Molodtsova, and P. Schuck, Experimental status of the nuclear spin scissors mode, Phys. Rev. C 97 (2018) 044316-(1–14). https://doi.org/10.1103/PhysRevC.97.044316.

[7] E. B. Balbutsev, I. V. Molodtsova, A. V. Sushkov, N. Yu. Shirikova, and P. Schuck, Spin-isospin structure of the nuclear scissors mode, Phys. Rev. C 105 (2022) 044323-(1–20). https://doi.org/10.1103/PhysRevC.105.044323.

[8] E. B. Balbutsev and I. V. Molodtsova, Scissors mode in transuranium elements, Eur. Phys. J. A 60 (2024) 185-(1–15). https://doi.org/10.1140/epja/s10050-024-01386-4.

[9] B. L. Berman and S. C. Fultz, Measurements of the giant dipole resonance with monoenergetic photons, Rev. Mod. Phys. 47 (1975) 713–761. https://doi.org/10.1103/RevModPhys.47.713.

[10] A. V. Varlamov, V. V. Varlamov, D. S. Rudenko, and M. E. Stepanov, Atlas of Giant Dipole Resonances, Parameters and Graphs of Photonuclear Reaction Cross Sections, INDC, Vienna, 1999.

[11] H. P. Morsch, P. Decowski, and W. Benenson, Fine structure in the giant resonance region and the collective dipole spin-flip excitation in ^{208}Pb, Nucl. Phys. A 297 (1978) 317–334. https://doi.org/10.1016/0375-9474(78)90279-8.

[12] H. Sagawa and B. Castel, The giant-dipole and spin-dipole resonances: A coexistence problem, Nucl. Phys. A 435 (1985) 1–6. https://doi.org/10.1016/0375-9474(85)90298-2.

[13] B. Castel and L. Zamick, New spin excitation modes in nuclei, Phys. Rep. 148 (1987) 217–247. https://doi.org/10.1016/0370-1573(87)90027-5.

[14] B. Castel and I. Hamamoto, Giant spin resonances and effective $M\lambda g$-factors, Phys. Lett. B 65 (1976) 27–30. https://doi.org/10.1016/0370-2693(76)90526-8.

[15] J. Kvasil, N. Lo Iudice, V. O. Nesterenko, A. Macková, and P. Alexa, Orbital and spin magnetic quadrupole response in heavy nuclei, Phys. Rev. C 63 (2001) 054305-(1–11). https://doi.org/10.1103/PhysRevC.63.054305.

[16] G. Kružić, T. Oishi, and N. Paar, Magnetic quadrupole transitions in the relativistic energy density functional theory, Eur. Phys. J. A 59 (2023) 50-(1–14). https://doi.org/10.1140/epja/s10050-023-00958-0.

[17] E. B. Balbutsev, J. Piperova, M. Durand, I. V. Molodtsova, and A. V. Unzhakova, Giant dipole resonance and other 1^- excitations, Nucl. Phys. A 571 (1994) 413–426. https://doi.org/10.1016/0375-9474(94)90219-4.

[18] E. B. Balbutsev, I. V. Molodtsova, and A. V. Unzhakova, Compressional and toroidal dipole excitations of atomic nuclei, Europhys. Lett. 26 (1994) 499–504. https://doi.org/10.1209/0295-5075/26/7/004.

[19] E.B. Balbutsev, I. V. Molodtsova, and J. Piperova, Collective 3^- and 2^- excitations with Skyrme forces, Sov. J. Nucl. Phys. 53 (1991) 670–679.

[20] E. B. Balbutsev and I. V. Molodtsova, Giant dipole and spin magnetic quadrupole resonances within Wigner function moments method, Int. J. Mod. Phys. E 35 (2026) 2641007-(1–12). https://doi.org/10.1142/S0218301326410077.

[21] P. Ring and P. Schuck, The Nuclear Many-Body Problem, Springer, Berlin, 1980.

[22] V. G. Soloviev, Theory of Complex Nuclei, Pergamon Press, Oxford, 1976.

[23] E. B. Balbutsev, L. A. Malov, P. Schuck, M. Urban, and X. Viñas, Nuclear scissors mode with pairing, Phys. At. Nucl. 71 (2008) 1012–1030. https://doi.org/10.1134/S1063778808060057.

[24] D. A. Varshalovitch, A. N. Moskalev, and V. K. Khersonski, Quantum Theory of Angular Momentum, World Scientific, Singapore, 1988.

[25] A. Bohr and B. R. Mottelson, Nuclear Structure, Vol. II, Benjamin, New York, 1975.

[26] T. Suzuki and D. J. Rowe, The splitting of giant multipole states of deformed nuclei, Nucl. Phys. A 289 (1977) 461–474. https://doi.org/10.1016/0375-9474(77)90046-X.

[27] J. Wambach and B. Schwesinger, Damping of highly excited vibrations in heavy nuclei, J. de Phys. 45 (1984) C4-281–C4-296. https://doi.org/10.1051/jphyscol:1984421.

[28] P. von Neumann-Cosel, N. Neumeyer, S. Nishizaki, V. Yu. Ponomarev, C. Rangacharyulu, B. Reitz, A. Richter, G. Schrieder, D. I. Sober, T. Waindzoch, and J. Wambach, Spin and orbital magnetic quadrupole resonances in ^{48}Ca and ^{90}Zr from 180° electron scattering, Phys. Rev. Lett. 82 (1999) 1105–1108. https://doi.org/10.1103/PhysRevLett.82.1105.

[29] I. Gheorghe, S. Goriely, N. Wagner, T. Aumann, M. Baumann, P. van Beek, P. Kuchenbrod, H. Scheit, D. Symochko, T. Ari-izumi, F. L. Bello Garrote, T. Eriksen, W. Paulsen, L. G. Pedersen, F. Reaz, V. W. Ingeberg, S. Belyshev, S. Miyamoto, and H. Utsunomiya, Photoneutron cross section measurements on ^{208}Pb in the giant dipole resonance region, Phys. Rev. C 110 (2024) 014619-(1–19). https://doi.org/10.1103/PhysRevC.110.014619.

[30] B. Wasilewska, M. Kmiecik, M. Ciemała, A. Maj, F. C. L. Crespi, A. Bracco, M. N. Harakeh, P. Bednarczyk, S. Bottoni, et al., γ decay to the ground state from the excitations above the neutron threshold in the ^{208}Pb$(p, p'\gamma)$ reaction at 85 MeV, Phys. Rev. C 105 (2022) 014310-(1–7). https://doi.org/10.1103/PhysRevC.105.014310.

[31] A. M. Lane, Nuclear Theory, Benjamin, New York, 1964.